Development/Plasticity/Repair

The Role of Protocadherin γ in Adult Sensory Neurons and Skin Reinnervation

Rebecca M. Long,[1] Honyi Ong,[1*] Wendy Xueyi Wang,[2,3*] Prashanth Komirishetty,[1] Aparna Areti,[1] Ambika Chandrasekhar,[1] Matt Larouche,[1] Julie L. Lefebvre,[2,3] and Douglas W. Zochodne[1]

[1]Division of Neurology, Department of Medicine and the Neuroscience and Mental Health Institute, University of Alberta, Edmonton, Alberta T6G 2G3, Canada, [2]Program for Neuroscience and Mental Health, Hospital for Sick Children, Toronto, Ontario M5G 1X8, Canada, and [3]Department of Molecular Genetics, University of Toronto, Toronto, Ontario M5R 0A3, Canada

The clustered protocadherins (cPcdhs) play a critical role in the patterning of several CNS axon and dendritic arbors, through regulation of homophilic self and neighboring interactions. While not explored, primary peripheral sensory afferents that innervate the epidermis may require similar constraints to convey spatial signals with appropriate fidelity. Here, we show that members of the γ-Pcdh (Pcdhγ) family are expressed in both adult sensory neuron axons and in neighboring keratinocytes that have close interactions during skin reinnervation. Adult mice of both sexes were studied. Pcdhγ knock-down either through small interfering RNA (siRNA) transduction or AAV-Cre recombinase transfection of adult mouse primary sensory neurons from floxed Pcdhγ mice was associated with a remarkable rise in neurite outgrowth and branching. Rises in outgrowth were abrogated by Rac1 inhibition. Moreover, AAV-Cre knock-down in Pcdhγ floxed neurons generated a rise in neurite self-intersections, and a robust rise in neighbor intersections or tiling, suggesting a role in sensory axon repulsion. Interestingly, preconditioned (3-d axotomy) neurons with enhanced growth had temporary declines in Pcdhγ and lessened outgrowth from Pcdhγ siRNA. *In vivo*, mice with local hindpaw skin Pcdhγ knock-down by siRNA had accelerated reinnervation by new epidermal axons with greater terminal branching and reduced intra-axonal spacing. Pcdhγ knock-down also had reciprocal impacts on keratinocyte density and nuclear size. Taken together, this work provides evidence for a role of Pcdhγ in attenuating outgrowth of sensory axons and their interactions, with implications in how new reinnervating axons following injury fare amid skin keratinocytes that also express Pcdhγ.

Key words: axon regeneration; peripheral sensory neurons; protocadherin γ; skin innervation

Significance Statement

The molecular mechanisms and potential constraints that govern skin reinnervation and patterning by sensory axons are largely unexplored. Here, we show that γ-protocadherins (Pcdhγ) may help to dictate interaction not only among axons but also between axons and keratinocytes as the former re-enter the skin during reinnervation. Pcdhγ neuronal knock-down enhances outgrowth in peripheral sensory neurons, involving the growth cone protein Rac1 whereas skin Pcdhγ knock-down generates rises in terminal epidermal axon growth and branching during re-innervation. Manipulation of sensory axon regrowth within the epidermis offers an opportunity to influence regenerative outcomes following nerve injury.

Received Oct. 14, 2022; revised Oct. 2, 2023; accepted Oct. 4, 2023.

Author contributions: R.M.L., H.O., P.K., A.A., A.C., M.L., J.L.L., and D.W.Z. designed research; R.M.L., H.O., W.X.W., P.K., A.A., A.C., M.L., and J.L.L. performed research; J.L.L. and D.W.Z. contributed unpublished reagents/analytic tools; R.M.L., H.O., W.X.W., P.K., A.A., A.C., M.L., J.L.L., and D.W.Z. analyzed data; R.M.L. and H.O. wrote the first draft of the paper; R.M.L., H.O., W.X.W., A.C., M.L., J.L.L., and D.W.Z. edited the paper; R.M.L. and D.W.Z. wrote the paper.

R.M.L was supported by a University of Alberta Faculty of Medicine and Dentistry Dean's Doctoral award. H.O. was supported by 75th Anniversary Award, Faculty of Medicine and Dentistry, University of Alberta. W.X.W. was supported by an Ontario graduate scholarship. J.L.L was supported by Canada Research Chair (Tier 2), a Sloan Fellowship in Neuroscience, a National Science and Engineering Research Council (NSERC) Discovery grant, and a Canadian Institutes of Health Research (CIHR) project grant. D.W.Z. was supported by the CIHR Project Grant File#362082. Trevor Poitras and Twinkle Joy offered methodological assistance, and Scott Stone and Nathan Wispinski offered statistical assistance.

*H.O. and W.X.W. contributed equally to this work.

The authors declare no competing financial interests.

Correspondence should be addressed to Douglas W. Zochodne at zochodne@ualberta.ca.

https://doi.org/10.1523/JNEUROSCI.1940-22.2023

Introduction

Successful reinnervation of target organs after axon injury requires both robust plasticity of the regenerating neuron but also receptivity of the target. Despite evidence that epidermal sensory axon terminals have inherent growth properties and plasticity, how they might be specifically welcomed back to the skin after injury has had limited attention.

When a peripheral nerve axon is injured, a cascade of events is initiated to prepare the neuron for regeneration and the disconnected stump for degeneration: the distal portion of the axon degrades through active molecular programs that are triggered by a drop in NMNAT2, involving SARM1, mPTP, and other calpains and proteases (Barrientos et al., 2011; Zochodne, 2012; Gerdts et al., 2013; Conforti et al., 2014), while the cell body

launches a regenerative response involving transcriptional changes, downregulating constitutively present genes while upregulating regeneration-associated genes (Verge et al., 1996; Senger et al., 2018). Schwann cells and macrophages create a microenvironment conducive for regeneration, providing trophic factors and phagocytic clearance of axonal debris including inhibitory by-products (Webber et al., 2011; Zigmond and Echevarria, 2019). Despite these events, reinnervation of skin sensation in the periphery retains substantial roadblocks (Zochodne, 2012), including the slow rate of regeneration and additional barriers posed by long distances to targets. Despite instances in which roadmaps are favorable, flawed axonal pathfinding adds an additional regenerative roadblock (Allodi et al., 2012).

Axonal rewiring involves adhesive and wiring specificity molecules, requirements less studied in peripheral nervous system (PNS) interactions between adult sensory axons and their regenerative targets in the skin. Clustered protocadherins (cPcdhs) are important candidates for these roles. Within olfactory and serotonergic developing neurons, this large family of cadherin-related molecules has been linked to an important role in influencing terminal endings and connections within sensory systems (Garrett et al., 2012; Lefebvre et al., 2012; Chen et al., 2017; Mountoufaris et al., 2017; Wu and Jia, 2021). For example, the γ subcluster (Pcdhγ) has been shown to be critical for proper isoneuronal avoidance (Lefebvre et al., 2012) which allows neurons to coordinate with their own dendritic arbor, and those of neighboring neurons. This ensures a reduction in the redundancy of innervation, a biologically costly endeavor, and separates or spaces out sensory receptors (Lefebvre, 2017). cPcdhs have also been shown to facilitate axon convergence, directing neurons to distinct olfactory glomeruli (Hasegawa et al., 2016; Mountoufaris et al., 2017), whereas the α subcluster (Pcdhα), has a similar role within serotonergic circuits (Chen et al., 2017). Meltzer et al. (2023) examined mice with a conditional Pcdhγ deletion and identified impairments in mechanosensitivity, and altered sensorimotor integration accompanied by altered synaptic function and morphology between somatosensory and dorsal horn neurons. In addition, these mice had reduced hair follicle innervation by Aβ low threshold mechanoreceptors and a decline in axonal branching associated with guard hairs.

Only recently has it been shown that peripheral sensory neurons, like their central counterparts, engage in topographic coordination of their projections with tiling and self-avoidance (Kuehn et al., 2019), although it is uncertain whether the Pcdhs participate. Further, whether these strategies are recruited following a peripheral nerve injury, involving re-navigation of axons to distant targets such as skin is unknown. Rewiring of skin with an appropriate recapitulation of axon investment is critical to regaining normal sensation.

Here, we provide evidence that the Pcdhγs are expressed in both adult sensory neurons and the epidermis, and that they influence axon growth and skin reinnervation. Moreover, we find evidence that the Pcdhγs not only influence outgrowth properties, but also self and neighbor interactions with new axons. The Pcdhγs are expressed in keratinocytes in the skin where it may fill an important role in patterning by inhibiting overabundant regrowth. In support of this, manipulation of Pcdhγ expression had a major impact on the extent of terminal epidermal regrowth during regeneration. Further understanding of this pathway in the sensory axons and their targets may yield new therapeutic targets for repair of denervated skin following injury or neuropathy.

Table 1. Forward and reverse primer sequences for qRT-PCR

GENE	FWD/REV	Primer Sequence (5′—3′)
RPLP0	FWD	AAGAACACCATGATGCGCAAG
	REV	TTGGTGAACACGAAGCCCA
Pcdhg-c3	FWD	CTCAGTGTGACTGATCTGGATG
	REV	GAGGGAAGAAGTCAGGCTAAAG
Pcdhg-c5	FWD	GCCTTATTGGAGGATGACTCTG
	REV	GTACTGTTGCTGTGGAGGATAG
Pcdhg-con	FWD	TGGCCCAACAACCAGTTTGA
	REV	AGGGTAAACTGGGGTCCGTA

Relative fold expression of mRNA was compared against the housekeeping protein, ribosomal protein lateral stalk subunit P0 (RPLP0) and was calculated using the comparative CT method ($2^{-\Delta\Delta CT}$).

Materials and Methods

Surgical preparation and animal care

Adult C57BL/6 mice of either sex between 30–180 d of age were used for all experiments, randomly allocated as available without specific age segregation. For *in vitro* studies, neurons with the floxed Pcdhg allele (*Pcdh-g*^{Fcon3}; Lefebvre et al., 2008; Prasad et al., 2008) were harvested from mice kindly donated by the Lefebvre laboratory, at the Hospital for Sick Children. All procedures and protocols were conducted in accordance with the guidelines established by the Canadian Council for Animal Care and were reviewed and approved by the Animal Care and Use Committee of the University of Alberta. Animals were housed in groups of five in individually ventilated cages with enrichment under a 12/12 h light/dark schedule and provided food and water *ad libitum*. Animals were killed through cardiac exsanguination under isofluorane anesthesia.

Peripheral nerve injury models

Mice were anaesthetized through 2% inhaled isofluorane until surgical plane was reached. The right hind leg was then shaved and disinfected. The sciatic nerve was exposed mid-thigh and crushed between forceps for 15 s in two orthogonal orientations. Mice were recovered and administered buprenorphine 0.25 mg/kg b.i.d for the following 3–5 d for postoperative pain management.

Pcdhg detection and quantification

qRT-PCR

Tissue was collected and placed into TRIzol reagent (Invitrogen) for RNA extraction following manufacturer's instructions. One microgram of total RNA was treated with DNase (Promega) to eliminate genomic DNA contamination. RNA was then subjected to a High Capacity cDNA Reverse Transcription kit (Applied Biosystems). Primer sequences used are listed under Table 1.

Immunohistochemistry

Following animal euthanasia, dorsal root ganglia (DRGs) from L4 to L6 and 1-cm sections of sciatic nerve taken from mid-thigh were harvested from each mouse and placed into a Modified Zamboni's fixative (2% paraformaldehyde and 0.5% picric acid in PBS) for 12–24 h at 4°C. DRGs and nerves were processed as described (Chandrasekhar et al., 2021). Tissue was rinsed with PBS and cryoprotected in a 20% sucrose/PBS solution for 24 h at 4°C. Tissue was then embedded in optimal cutting compound (OCT) and cut into 12-µm-thick sections using a cryostat. Sections were mounded onto electrostatically charged slides (Thermo Fisher Scientific) and left to dry. Sciatic nerves were cut transversely.

DRG and nerve sections were blocked using a solution containing 10% normal goat serum, 1% bovine serum albumin (BSA), 0.3% Triton X-100, and 0.05% Tween 20 for 1 h at room temperature (RT). Sections were then incubated in the primary solution containing primary antibodies (1:200, mouse anti-NF200, Millipore catalog #MAB5266, RRID: AB_2149763, 1:500 rabbit anti-Pcdhg, Synaptic Systems catalog #190103, RRID: AB_2100954) in 1% normal goat serum, 0.1% BSA, 0.3% Triton X-100, and PBS overnight at 4°C. Slides were rinsed for 3 × 5 min in PBS, then incubated in the secondary solution (1:100 Alexa Fluor goat anti-rabbit 488 Thermo Fisher Scientific catalog #A32731TR, RRID: AB_2866491, 1:200

Alexa Fluor goat anti-mouse 546 Thermo Fisher Scientific catalog #A-11030, RRID: AB_2534089) for 1 h at RT. Sections were then rinsed 3 × 5 min and mounted with Vectashield Mounting Media (Vector Laboratories), coverslipped, and sealed.

Footpad samples were collected using a 3-mm biopsy punch and placed in 2% PLP [paraformaldehyde (2%), l-lysine, and sodium periodate] for 12–24 h at 4°C. Footpad processing and immunohistochemistry for PGP9.5 was conducted as previously described (Poitras et al., 2019). Biopsies were briefly rinsed and cryoprotected using a 20% glycerol/0.1 M Sorenson phosphate buffer solution for 24 h at 4°C. Biopsies were then embedded in OCT and cross-sectioned at 25 µm and mounted onto electrostatically charged slides (Thermo Fisher Scientific). Footpad sections underwent antigen retrieval in 65°C Tris-EDTA buffer for 90 min to encourage antigen presentation of PGP9.5, a marker for visualizing epidermal sensory fibers (Cheng et al., 2010). Sections were blocked in a solution of 10% normal goat serum, 1% BSA, 0.3% Triton X-100, and PBS for 1 h at RT. Sections were then incubated in a primary solution of 1% normal goat serum, 0.1% BSA, 0.04% EDTA, 0.3% Triton X-100, and the primary antibody (1:500 rabbit anti-PGP9.5 EnCor Biotechnology catalog #RPCA-UCHL1, RRID: AB_2210932) overnight at 4°C. Sections were then rinsed 3 × 5 min in PBS, and incubated in the same solution as above but with the secondary antibody in place of the primary (1:1000 Alexa Fluor goat anti-rabbit 546 Thermo Fisher Scientific catalog #A-11035, RRID: AB_2534093) for 1 h at RT. Sections were rinsed in PBS for 3 × 5 min and mounted with Vectashield, coverslipped, and sealed. Footpads, DRGs and sciatic nerves were imaged using a Leica SP5 confocal microscope. Confocal Z-stack images of stained footpad sections were obtained using a step size of 0.5 µm. For each section, five consecutive frames were imaged and this was repeated over three randomly chosen sections on the slide.

Confocal images were processed using ImageJ and epidermal innervation of footpads were analyzed in a blinded fashion for: (1) number of axons per mm^2 (per epidermal area), (2) number of axons per mm (per epidermal length), (3) number of vertical axons per mm, (4) number of horizontal axons per mm, iv) number of branching neurites from vertical axons, (5) interfiber distances (10–30 µm/short; 30–50 µm/medium; >50 µm/long), (6) number of dermal axons, (7) number of vertical dermal axons, (8) number of horizontal dermal axons, (9) number of DAPI-stained nuclei per mm^2 (per epidermal area), (10) number of DAPI-stained nuclei touching or in close contact (<10 µm) with axons, (11) number of DAPI-stained nuclei in close contact per mm of axons, and (12) DAPI-stained cell size. Both axon numbers per length and area were included for comparison to both previous data and to human work using numbers per length as a standard. Separately assessing axon trajectories by counting vertical and horizontal axons addresses directionality of epidermal axons. Vertical axons were defined as those that showed 45° to 90° angle deviation from the dermal/epidermal border. Horizontal axons were defined as those that showed 0° to 45° angle deviation from the dermal/epidermal border. Similar horizontal and vertical nerve fibers classifications were also applied for dermal axon analyses. Separate analysis was conducted to analyze dermal innervation. For dermal analyses, only axons that were identified to within 50 µm beneath the dermal/epidermal border were counted. Finally, assessments of epidermal structure were conducted focusing on nuclear keratinocyte staining (for clarity in identifying traversing axons) and its relationship to axons. For number of DAPI-stained nuclei per area, a minimum of 50 µm was traced across the superficial epidermal border and all the DAPI-stained nuclei beneath the traced line was counted and divided by the thickness of the traced epidermis area. For the number of DAPI-stained nuclei in close contact with axons, only those DAPI-stained cells that were within 10 µm from the axons, based on an estimate of keratinocyte mean diameter, were counted to address interactions between axons and keratinocytes. For DAPI-stained cell size, 100 randomly selected DAPI-stained cell nuclei were traced per footpad for determination of the mean nuclear areas (μm^2).

Western immunoblot. Protein was extracted from DRG and footpad tissues and quantified using the Bradford assay. Twenty-five ug of denatured protein lysate was loaded into each well of a gel. The gel was run at 75 V until the protein bands reached the 7.5% resolving gel, at which point the voltage was adjusted to 100 V until the bands reached the bottom of the gel. Proteins were transferred to a PVDF membrane over 90 min at 100 V. Membranes were then blocked in a solution containing 5% BSA in TBST. Membranes were incubated for the presence of Pcdhγ (1:1000 rabbit anti-Pcdhγ, Synaptic Systems) in 5% BSA/TBST overnight at 4°C. β-Actin was used as a loading control (1:3000 rabbit anti-β-actin primary, Abcam). Blots were visualized using goat anti-rabbit HRP (1:3000 Life Technologies). Large differences in band intensity between low intensity Pcdhγ and high intensity actin required separate exposure, precluding densitometry measures from the same blot (not reported).

Single-molecule fluorescence in situ *hybridization (smFISH).* Hybridization chain reaction (HCR) amplification-based smFISH was performed following previous methods (Moffitt and Zhuang, 2016; Choi et al., 2018; W.X. Wang and Lefebvre, 2022; Moffitt et al, 2016). Briefly, wild-type mouse DRGs and footpads were sectioned at 25 μm onto 12-mm silane-treated coverslips. Primary probes targeting the *Pcdhg* constant region or C isoform variable region was performed at 2 nM probe concentration in HCR hybridization buffer (Molecular Instruments) at 37°C overnight; 4% polyacrylamide gels were cast for tissue clearing according to previous descriptions (Moffitt and Zhuang, 2016; Moffitt et al, 2016). Gels were incubated for 30 min at 4°C, before gelation at 37°C for 2 h. Tissue clearing occurred for 1.5 h at 37°C in clearing buffer consisting of 1:100 proteinase K, 50 mM $Triss^2HCl$ pH 8.0, 1 mM EDTA, 0.5% Triton X-100, 500 nM NaCl, and 1% SDS. After clearing, samples were washed 3× in 2× SSCT before HCR amplification. HCR amplification occurred at room temperature for 12–18 h. Probe panels were designed with a 25 nt targeting region using the following parameters: (1) GC content between 45–70%; (2) does not contain five or more consecutive nucleotide bases of the same kind; (3) no more than 14 nt of consecutive match to any other transcript. C isoform probe sets contained 28 probes each. Pan-Pcdhg probe set contained 14 probes. Cell type-specific probe sets were purchased from Molecular Instruments.

siRNA-mediated knock-down model. Five microliters of small interfering RNA (siRNA) combined with HiPerfect Transfection reagent (QIAGEN) was applied directly to the sciatic nerve following axotomy. The wound was sutured, and the site was electroporated with 5 × 25-V pulses lasting 50 ms each, delivered at 1 Hz with an ECM830 Electro Square Porator unit. A total of 3 µl of siRNA was also injected subcutaneously to the plantar surface of the ipsilateral hind paw, and electroporated as above. Injections were repeated at both sites three times a week for 28 d (12 injections total).

Cell culture. For siRNA studies, uninjured mice or those with a 72-h prior axotomy were killed and the L4, L5, and L6 DRGs were removed from both the contralateral and ipsilateral side to the injury. DRGs were then dissociated and used for sensory neuron cultures using previously described methods (Poitras et al., 2019), with one modification of using 1% collagenase D for 30 min (Roche Applied Science) in L-15 media (Invitrogen) instead of 0.1% for 60 min, an approach generating greater cellular yield. For siRNA mediated knock-down cultures, 20 nM siRNA (sequences in Table 1; QIAGEN) was mixed with HiPerfect Transfection reagent (QIAGEN) 15 min before adding to the culture media. Uninjured cultures were incubated at 37°C for 72 h with siRNA treatment, and previously axotomized neurons were incubated for 24 h because of their accelerated growth following conditioning. Cells were fixed using a 4% PFA solution, rinsed for 3 × 5 min in PBS, and blocked with 5% BSA and 0.3% Triton X-100 in PBS for 1 h at RT. Cells were then incubated in 3% BSA, 0.3% Triton X-100, and the primary antibody (1:200 rabbit anti-NF200, Sigma-Aldrich catalog #N4142, RRID: AB_477272) for 75 min at RT. They were rinsed as above and incubated in the secondary antibody (1:200 Alexa Fluor goat anti-rabbit 488 Thermo Fisher Scientific catalog #A32731TR, RRID: AB_2866491) in a solution with 3% BSA and 0.3% Triton X-100. Cells were mounted using Vectashield mounting media with DAPI and imaged using a Zeiss AxioScope at 20×.

AAV-Cre mediated knockdown models. For AAV-Cre knock-down, DRGs (15–20) were harvested from C57BL/6 mice of both sexes with the genotype $Pcdhg^{flox/flox}$ kindly donated by the Lefebvre laboratory from the University of Toronto. Cell cultures were split evenly into two groups: (1) those that received AAV-iCre-mCherry (Pcdhγ knock-down group), (2) those that received AAV-mCherry (control group).

AAV-iCre-mCherry or AAV-mCherry (Vector Biolab) were mixed with the cell culture media before seeding at a virus concentration of 500 plaque forming units (PFU). Cell cultures were then incubated at 37°C for 24 h to allow for transfection and after a day, were fixed for analysis. Mouse DRGs (15–20 count) were harvested and placed into cold L-15 media. DRGs were rinsed twice, 2 min each, using fresh L-15 and placed into 1% collagenase D (Roche Applied Science) dissolved in L-15 and incubated at 37°C for 60 min. Following collagenase D digestion, DRGs were resuspended through trituration to ensure they dissociate into a single-cell clear suspension. This single-cell suspension was centrifuged at 800 rpm for 6 min at room temperature. The pellet of DRGs was then resuspended in fresh L-15 and poured through a 70-μm mesh, recentrifuged again and the pellet resuspended in fresh L-15 and passaged through a 15% BSA gradient to separate out tissue debris and Schwann cells (supernatant) from the neurons (pellet). Finally, the pellet was resuspended in fresh culture media containing DMEM (Invitrogen), N-2 supplement (Invitrogen), NGF (Invitrogen), cytosine-β-arabinofuranoside (Sigma-Aldrich), and penicillin and streptomycin. DRG cell cultures were then incubated for 24 h at 37°C. Neurons were administered 0.5 µl of AAV2-mCherry-iCre or AAV2-mCherry (Vector Biolabs) combined with 1 ml of DPBS (Dulbecco's phosphate buffered saline) with 5% glycerol and kept at 4°C. Before DRG cell culture plating, 5 µl of AAV-mCherry-iCre or AAV2-mCherry in DPBS with 5% glycerol were mixed with DRG cell culture medium. DRG cell culture media containing AAV2-mCherry-iCre or AAV2-mCherry were then mixed with DRG cells and plated onto chamber slides. DRG cell culture was then incubated for 24 h at 37°C before fixing. Cell cultures were fixed using 4% paraformaldehyde in PBS. To prevent osmotic shock, 500 μl of culture media was removed from each chamber and replaced with 4% paraformaldehyde in PBS for 5 min. Following that, all remaining solution was removed from each chamber and cells were again fixed with 600 μl of 4% paraformaldehyde in PBS for 10 min. Before blocking, DRG culture was rinsed with PBS three times, 5 min each. Blocking was then conducted using 30% normal goat serum in PBS for 30 min. As above, DRGs were stained with a primary antibody (1:500 mouse monoclonal anti-β-tubulin III, Millipore Sigma catalog #T8660) for 75 min at a concentration ratio of 1:500. Following primary antibody staining, cell cultures were rinsed three times with PBS, 5 min each before staining with secondary antibody (1:500 Alexa Fluor goat anti-mouse 488 Thermo Fisher Scientific catalog #A28175, RRID: AB_2536161) for 75 min. For both the primary antibody and secondary antibody staining, the DRGs were incubated in a solution containing 0.3% Triton X-100, 0.1% normal goat serum and PBS. After secondary antibody staining, the cell cultures were rinsed three times with PBS, 5 min each and then mounted with Vectashield DAPI-containing mounting media, coverslipped and finally sealed. To determine whether the cells were successfully transfected, DRGs were also stained with an mCherry antibody (1:500 recombinant rabbit anti-mCherry antibody, Abcam, catalog #ab213511, RRID: AB_2814891) and then labeled with Alexa Fluor546 goat anti rabbit antibody. As a further confirmation of Pcdhγ knock down (KD), in-cell western assays were performed. DRG neurons were cultured and plated on a 96-well plate. Neurons from a single mouse were divided into two columns/groups: (1) Pcdhγ KD group that received AAV-iCre-mCherry, (2) control group that received AAV-mCherry. The plate was incubated at 37°C for 24 h and following that, DRGs were fixed and permeabilized using methanol. After fixation, DRGs were rinsed twice with PBS, 2 min each. Next, the wells were incubated with Li-Cor Intercept blocking buffer (Li-Cor) for 1 h at room temperature. Wells were then incubated with 1:100 mouse anti-Pcdhγ antibody (Santa Cruz) diluted in Li-Cor blocking buffer overnight at 4°C. After primary antibody incubation, wells were rinsed with phosphate buffer saline with Tween detergent (PBST) for three times, 5 min each. After rinsing, DRGs were stained with secondary antibody solution composed of 1:1000 goat anti-mouse Dylight 800 antibody (Invitrogen) diluted in Li-Cor blocking buffer for 1 h at room temperature. Wells were once again rinsed with PBST and distilled water was added. Finally, the plate was analyzed using a Li-Cor Odyssey CLx infrared scanner. For these experiments, the intensity of staining from each well within a column was averaged and used for statistical analyses.

Dissociated DRG sensory neurons studied in the setting of Rac1 inhibition were prepared as above into four groups: (1) those that received AAV-iCre-mCherry, (2) those that received AAV-iCre-mCherry + Rac1 inhibitor, (3) those that received AAV-mCherry, and (4) those that received AAV-mCherry + Rac1 inhibitor. AAV-iCre-mCherry or AAV-mCherry was mixed with the cell culture media before seeding at a virus concentration of 500 PFU. Rac1 inhibitor (NSC-23766; Focus Biomolecules) was added to the cell culture media for (2) and (4) groups at concentrations of 5–50 mg/ml. Cell cultures were then incubated at 37°C for 24 h and fixed.

Neurite outgrowth analysis. For the siRNA studies, each neuron was imaged alone to maximize accuracy of the neurite tracing software, Neuromath (Rishal et al., 2013). Sholl analyses were conducted using the ImageJ (NIH) Sholl plugin, with a shell size of 10 µm and manually identified soma centers. Intraneuronal and interneuronal neurite intersections were analyzed manually offline. For interneuronal intersections, randomly selected images containing two nearby neurons were chosen, provided they contained neurons that exhibited neurites growing toward the other cell body and were only included if the length of the longest neurite could intersect with the longest neurite emerging from the other neuron. As well, the branching complexity of each DRG neuron was measured. For the neighboring crossing analysis, images containing two DRG neurons with their respective neurite outgrowth were captured. Self-crossings are defined as those neurites arising from the same nucleus overlapping or intersecting one another, while interneuronal, or neighboring axon crossings are defined as those neurites arising from different nuclei overlapping or intersecting one another. Self-crossings were counted manually. A total of 600 neurons (300 for AAV-iCre-mCherry group, 50 per culture; 300 for AAV-mCherry group, 50 per culture) were studied for their self-crossings (intraneuronal interactions). Neighboring crossings were counted similarly using a total of 600 DRG neurons (41 for AAV-iCre-mCherry group; 36 for AAV-mCherry group).

Electrophysiology and behavior measures. Sensory and motor multifiber conduction measurements were conducted as previously described (Poitras et al., 2019) at baseline, 14 d, and 28 d postinjury. Mice were maintained under isofluorane anesthesia while maintaining near nerve temperature at 37°C. Sensory nerve action potentials (SNAPs) were recorded at the popliteal fossa, following stimulation of the digital sensory nerves within the hindpaw and averaged over 10 consecutive recordings filtered between 10 and 2 kHz. Compound motor action potentials (CMAPs) and nerve velocities were measured from recordings from two separate sites, by stimulating the sciatic notch and the knee and recording at the hindpaw. The signal was filtered between 10–10 kHz.

Mice were also tested for thermal and mechanosensitivity at the same timepoints using the Hargreaves apparatus and Von Frey fibers as previously described (Poitras et al., 2019). Animals were acclimated before testing. To test thermal sensitivity, mice were placed on a Plexiglas platform with a radiant heat source applied to the middle plantar aspect of either hind paw, and the latency to withdraw the paw was recorded. Trials were averaged per paw, with time between trials to allow the footpad sensation to normalize. Von Frey fibers were used to test mechanosensitivity, and fibers ranging from 0.4 to 4 g were used. Starting from the lowest, fibers were applied in increasing weights until the fiber elicited a response 75% of the time, which was then recorded as the mechanical pain threshold. If there was no response following five trials, the next weight up was used until a response was elicited. If no response was elicited at 4 g, the recorded threshold was 4 g.

Statistical analyses. Statistical analyses were conducted using GraphPad Prism 8 (RRID: SCR_002798), JASP (RRID: SCR_015823), and MATLAB software (RRID: SCR_001622) using appropriate parametric and nonparametric tests. Sample sizes were based on prior experience with each of the models. Comparisons were checked with nonparametric statistics if the sample size was less than four, or the data fell in a non-normal distribution. For *in vitro* studies, both paired and unpaired analyses were conducted but paired studies were justified by the experimental approach. Each culture, based on one to

two DRG was paired with samples taken on the same day, from the same animal and treated identically with the exception of the experimental intervention. One culture day was considered an $n = 1$, averaging quantitated results from all the neurons examined. For groups of more than two, ANOVA or nonparametric Friedman's tests were routinely applied as well as occasional, strictly selected and relevant (*ad hoc*) two-way comparisons as described. Two-tailed Student's *t* tests were usually employed but in selected instances where a direction of change was anticipated, we justified occasional use of one-tailed tests, as indicated. For *in vivo* studies, selected analyses were made in the same mouse ipsilateral and contralateral to nerve injury. For these mice paired *t* tests were applied within the groups. Values were reported as mean ± SEM.

Results

Pcdhγ is expressed within the mammalian peripheral nervous system

The Pcdhγ subfamily comprises 22 isoforms that are each encoded by a distinct "variable" exon spanning the extracellular and juxtamembrane domains along with three "constant" exons encoding the intracellular region and shared by all isoforms (Wu et al., 2001). A pan-Pcdhγ antibody targeting the constant region confirmed protein expression within DRG sensory neuron cytoplasm, but not nuclei, in both mouse and rat compared with a primary negative control (Fig. 1*A*,*C*) confirming previous reports using a knock-in mouse line in which endogenous Pcdhγs were tagged with GFP (X. Wang et al., 2002; Prasad and Weiner, 2011). Pcdhγs were broadly expressed in all subtypes of DRG neurons and were not limited to a specific subtype, such as Nf200 which is more prominent in larger caliber neurons (Webber et al., 2011). Labeling of the footpad for Pcdhγ identified staining of keratinocytes (Fig. 1*B*). To detect expression of individual isoforms, primers were designed to target two C-type transcripts, gC3 and gC5, for initial qRT-PCR detection within peripheral tissue, as the three C-type isoforms are thought to be expressed more widely (Kaneko et al., 2006). Investigations of the dorsal root ganglion (DRG), sciatic nerve, and terminal sensory endings within the mouse footpad resulted in positive relative fold mRNA expression (Fig. 1*D*). Immunohistochemical analysis with corrected total cell fluorescence compared with a negative control where the primary antibody was omitted also confirmed low level sciatic nerve axonal expression (Fig. 1*E*,*F*) but expression in terminal axons was not resolved. Schwann cell expression was not observed.

Because of the role of the Pcdhs during development and its impact on guiding growing neurites shown in the CNS (Chen et al., 2012; Ing-Esteves et al., 2018; Flaherty and Maniatis, 2020), we investigated whether the Pcdhγs were altered following an injury, perhaps to assist in guiding regenerating axons in the PNS. We induced a sciatic nerve injury in mice and examined mRNA levels at several time points postinjury (Fig. 1*G*,*H*). We noted a consistent drop in the Pcdhg signal in both the gC3 and gC5 mRNA transcripts in the ipsilateral DRG compared with contralateral DRGs. Western immunoblot confirmed the presence of the Pcdhγ band at 100 kDa of low intensity and a qualitative decline in protein at 36 h in the DRG, but not in the footpad ipsilateral to injury (Fig. 1*I*–*K*). Western immunoblot quantitation did not identify a significant difference in the DRG or footpad of the protein at 36 h despite the trend observed. Keratinocyte Pcdhγ colocalization with keratin-5 and keratin-1 was confirmed in additional colabeling experiments (Fig. 1*L*–*N*).

Single-molecule fluorescence *in situ* hybridization (smFISH) using probes targeting the constant Pcdhg domain confirmed Pcdhg expression in the DRG cytoplasm as well as the epidermal layer of the footpad (Fig. 2*A*,*B*). Using isoform-specific probes, we confirmed robust expression of C-type Pcdh-gC3, gC4, and gC5 transcripts in DRG neurons (Fig. 2*A*). Interestingly, we observed isoform specific enrichment of Pcdhgs, such that a subset of cells displayed a visible reduction in Pcdhg*C4* mRNA (Fig. 2*A*, inset). To determine that the Pcdhgs are expressed by neuronal DRG subtypes, we mined an existing single-cell RNA sequencing (scRNA-Seq) dataset for the mouse DRG (Nguyen et al., 2021), and identified four cell-type markers (Pvalb, Ptprt, SST, and Gad2), to label four subpopulations (proprioceptive, nociceptive, pruriceptive, and mechanoreceptive sensory neurons, respectively) within the DRG. We confirmed Pcdhγ expression within individual DRG subtypes as well as single isoform expression (Fig. 2*C*, inset; showing PcdhgC3 expression in Pvalb+ proprioceptive neurons). Taken together, these findings indicate that Pcdhγ transcripts and protein were present in the peripheral nervous system, expressed highly in the DRG cytoplasm. Additionally, expression of Pcdhg transcripts and proteins were present within the keratinocytes in the skin, indicating that the Pcdhγs may play a role in neuron-keratinocyte interactions (Fig. 2*B*).

Pcdhγ siRNA knock-down enhances neurite extension of sensory neurons *in vitro*

There is abundant support for a role of Pcdhγ in dendritic arborization (Garrett et al., 2012; Lefebvre et al., 2012; Suo et al., 2012; Wu and Jia, 2021), but while there is evidence of their expression in DRGs (Prasad and Weiner, 2011), their impact on regenerating PNS axons is less studied. As in previous work (Duraikannu et al., 2018; Krishnan et al., 2018; Poitras et al., 2019), we designed a pan-Pcdhg small interfering RNA (siRNA) to knock down functional Pcdhγ in adult sensory neurons *in vitro*. qRT-PCR identified knock-down of the Pcdhg gene transcript after 72-h incubation compared with a Scrambled siRNA treatment (Fig. 3*A*). Pcdhγ knock-down neurons had an increase in the average overall neurite extension and branching points (Fig. 3*B*–*F*), suggesting an increase in complexity. Pcdhγ knock-down neurons also exhibited a nonsignificant trend toward hosting the longest branch. Finally, 55% of cultured neurons sprouted (exhibited at least one neurite from the soma) following Pcdhγ knock-down, compared with 42% following Scrambled siRNA treatment. Figure 3*B* shows example micrographs of the outgrowth of wild-type uninjured neurons treated with Pcdhγ siRNA (top row) and Scrambled siRNA (bottom row). The overall findings offered evidence that Pcdhγ has a role in the ongoing suppression of adult neuron plasticity.

We next addressed whether Pcdhγ also restrained outgrowth in preconditioned neurons known to exhibit enhance outgrowth (Senger et al., 2018), keeping in mind the declines in its expression we identified after injury. We analyzed average neurite outgrowth of neurons having undergone a prior 3d conditioning crush injury before harvesting (Injured, Inj; axotomy), These cultures were examined 24 h after plating because of the accelerated growth seen in injured neurons, compared with contralateral harvested neurons. Increased neurite outgrowth in response to Pcdhγ siRNA was not observed following injury (Fig. 3*G*–*J*) and also was no longer apparent in contralateral Pcdhγ KD neurons. Interestingly, while injured neurons from both siRNA groups generally had longer branches (Fig. 3*H*), Pcdhγ siRNA-treated neurons had reduced numbers of branching points (Fig. 3*I*).

To further evaluate the relationship between Pcdhγ knock-down and the neuron injury phenotype, we conducted a Sholl analysis to further evaluate neurite complexity (Fig. 3*J*–*L*). By placing concentric shells at 10 μm intervals from the center of a cell soma, we counted the number of neurites crossing at each

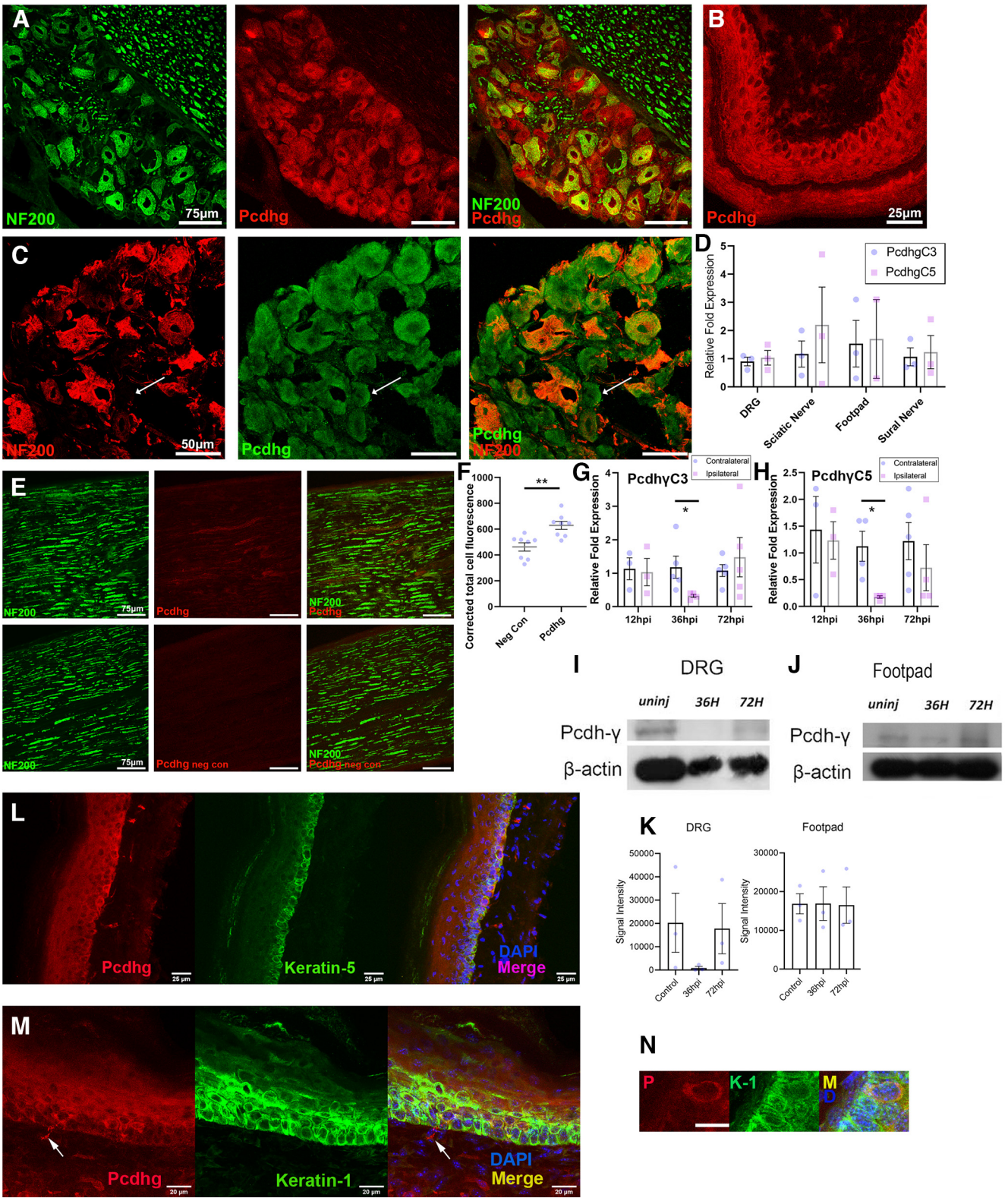

Figure 1. Pcdh γ protein and mRNA is expressed in the mammalian peripheral nervous system. Transverse sections of mouse (***A***) and rat (***C***) DRGs immunostained for NF200 and Pcdh γ. Arrow indicates a smaller diameter neuron positive for Pcdh γ but negative for NF200. Pcdh γ is also expressed in keratinocytes in transverse sections of mouse footpads (***B***). DRG, sciatic nerve, footpad, and sural nerve were all positive for mRNA transcripts of the gC3 and gC5 exons (***D***). Sciatic nerve showed low intensity expression of Pcdh γ compared with a negative control and quantitated (***E***, ***F***). (***F***; $^{**}p = 0.0022$, two-tailed Student's t test, $n = 8$/group). PcdhgC3 (***G***) and gC5 (***H***) mRNA transcripts in DRGs show a significant drop in expression 36 h on the ipsilateral side postinjury but return to normal levels by 72 h [(***G***) Pcdh γC3 $^{*}p = 0.02$ contra vs ipsi PcdhgC3 36 h, two-tailed Mann–Whitney, $n = 5$ contra, 4 ipsi; (***H***) PcdhgC5 $^{*}p = 0.026$ contra vs ipsi Pcdh γC3 36 h, two-tailed Mann–Whitney, $n = 4$/group]. Representative tissue western immunoblots (***I***, ***J***) with quantitation (***K***) from intact DRGs and footpads and ipsilateral to axotomy injury at 36 and 72 h (values not significantly different). DRG, dorsal root ganglion; NF200, neurofilament heavy subunit. Images of coexpression of keratin-5 (***L***) and keratin-1 (***M***, ***N***, higher power) with Pcdh γ confirming Pcdh γ colocalization within keratinocytes (arrow in ***M*** shows an axon also staining). Scale bar = 25 μm for ***L***, 20 μm for ***M***, and 10 μm for ***N***.

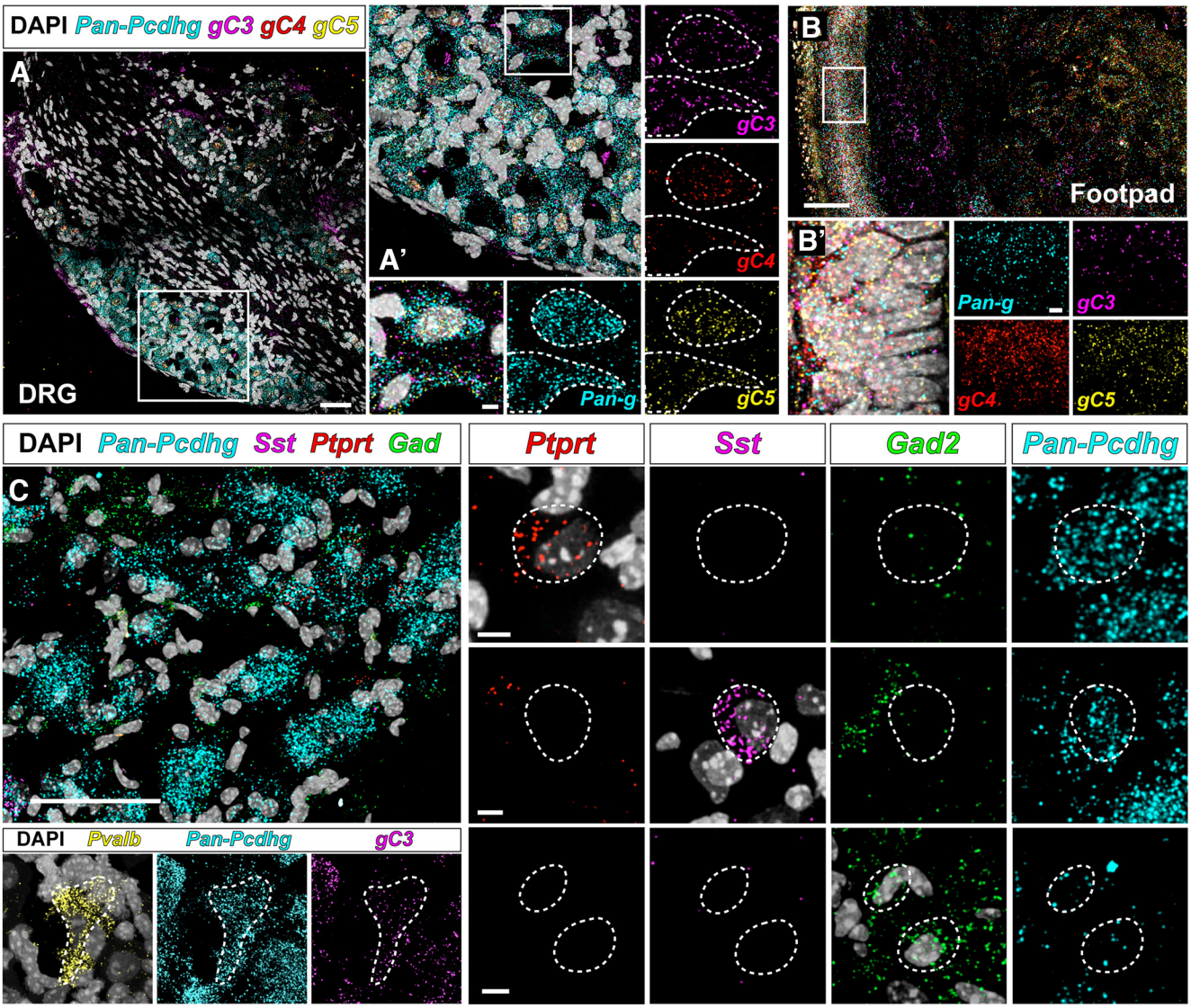

Figure 2. Pcdhg mRNA subtypes are expressed in DRG sensory neurons and skin. *In situ* hybridization of Pcdhg mRNA isoforms in both DRG and epidermal sections, with preferential expression of isoforms in certain types of mechanoreceptors. Pcdhγ isoforms are present in the cell bodies of peripheral sensory neurons, including the constant isoforms gC3, gC4, and gC5 (gC3,4,5; ***A***). The epidermis also shows hybridization of isoforms, with an increase in staining of the gC4 and gC5 isoform (***B***). ***A′***, ***B′***, Increased magnification of boxes in ***A***, ***B***. In neuronal DRG cells expressing Ptprt or Sst, there is an increase in pan-Pcdhγ staining, but relatively low in Gad2+ cells. There was also limited hybridization of the gC3 isoforms in Pvalb+ cells (***C***), in addition to other Pcdhγ isoforms. Scale bars in ***A–C*** are 50 μm, magnified images are 5 μm. ptprt, receptor-type tyrosine-protein phosphatase T; sst, somatostatin; Gad2, glutamate decarboxylase 2; pvalb, parvalbumin.

shell distance to quantify the extent of arborization. A two-way ANOVA identified a main effect of injury ($F_{(1,170)} = 19.317$, $p < 0.001$) based on the aggregate data in Figure 3*K*. Bonferroni pairwise comparisons indicated that this effect is likely driven by the difference between the injured Pcdhγ KD group (ipsilateral) and its uninjured contralateral) group. Notably, the Scrambled siRNA control group also differed from the Scrambled siRNA injured group also contributing to the findings that identified fewer crossings following injury. Average areas under the curve of four experiments are shown in Figure 3*L*. There was no significant impact of siRNA treatment but injury itself decreased the number of shell crossings at early lengths of outgrowth. Overall, these findings indicate that Pcdhγ does not suppress growth of adult preconditioned neurons that already have heightened growth. This may be a consequence of a decline in expression of Pcdhγ at the same time point analyzed, as suggested in Figure 1. However, in this setting, Pcdhγ may paradoxically act to heighten, rather than suppress proximal branching, which was reduced by its KD.

Conditional knock-down of Pcdhγs with AAV-Cre recapitulate enhanced neurite extension of uninjured sensory neurons *in vitro*

As an additional confirmation over neurite outgrowth behavior in the setting of Pcdhγ knock-down, we studied uninjured adult mouse DRG neurons harvested from *Pcdhg*$^{Fcon3/Fcon}$ mice (Lefebvre et al., 2008; Prasad et al., 2008) transduced with AAV-iCre-mCherry or AAV-mCherry vectors. These neurons were incubated for 24 h after plating. Neurons exposed to the AAV-Cre vector had greater neurite extension per neuron, neurite length, branching points and sprouting (Fig. 4*A*,*G*). Protein knock-down was confirmed by both western in-cell analysis (Fig. 4*B–D*) and fluorescent intensity during immunocytochemistry (Fig. 4*E*, illustrated in *F*).

An interaction between Pcdhγ and Rac1 has been previously identified, where a constitutively active Rac1 rescues dendritic morphogenesis defects following knock-down of Pcdhα and Pcdhγ clusters in the CNS (Suo et al., 2012). Given this, we evaluated whether enhanced growth in uninjured neurons exposed

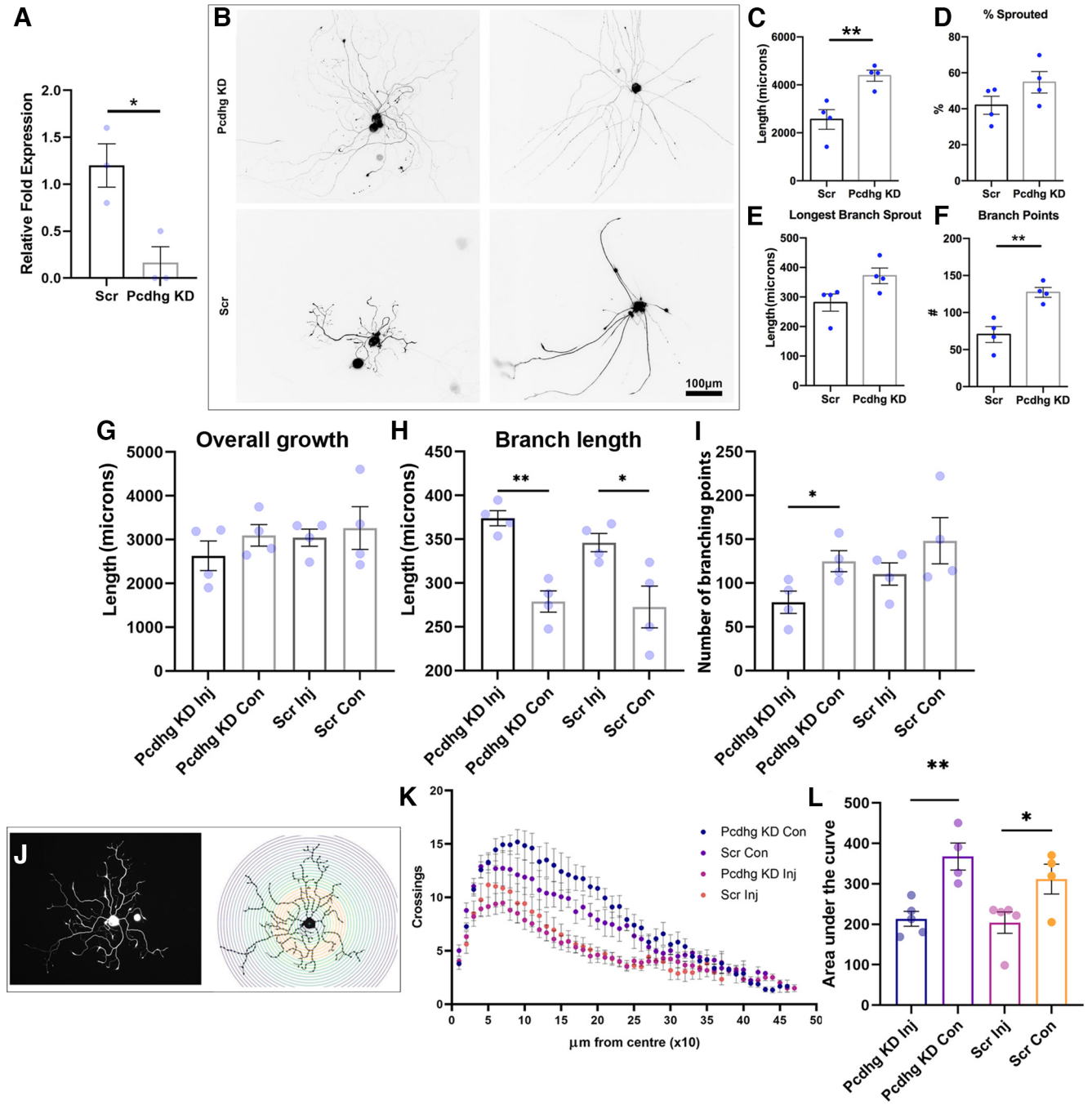

Figure 3. Pcdh γ siRNA knock-down *in vitro* alters axon outgrowth in naive but not injured adult sensory neurons. Confirmation of Pcdh γ mRNA knock-down *in vitro* by siRNA compared with Scrambled siRNA [***A***, mRNA Pcdh γ siRNA, $^{*}p = 0.04$, Pcdh γ KD vs scrambled control siRNA (Scrambled siRNA); one-tailed Mann–Whitney $n = 3$/group (alternately tested as $p = 0.02$ two-tailed unpaired Student's t test)]. Representative images of uninjured Pcdh γ siRNA-treated neurons (top row) and Scrambled siRNA siRNA-treated neurons (bottom row) following a 72-h incubation (***B***). The neurons depicted have an outgrowth average close to the mean of the respective groups. Analysis of neurite outgrowth (***C–F***) in naive uninjured DRG sensory neurons indicated longer average neurite outgrowth per neuron in the Pcdh γ siRNA group and greater numbers of branch points [(***C***) length of neurite outgrowth, $^{**}p = 0.0083$, Pcdh γ KD vs Scrambled siRNA; and (***F***) branchpoint numbers, $^{**}p = 0.0041$, Pcdh γ KD vs Scrambled siRNA; two-tailed unpaired Student's t tests; $n = 4$/group]. Neurite outgrowth was also examined in DRG neurons following a prior axotomy injury (72 h before culture) and their contralateral controls examined 24 h after plating (***G–I***). In contrast to the naive uninjured neurons above, increased neurite outgrowth was not identified either ipsilateral or contralateral to injury in response to Pcdh γ siRNA (***G***; overall neurite outgrowth). However, axotomy injury induced neurons to grow longer branches (***H***; individual branch length) and in the case of Pcdh γ KD neurons, fewer branching points [***I***; (***H***) for longest branch length, $p = 0.0009$ ANOVA, *post hoc*, $^{**}p = 0.0007$ Pcdhg KD Inj vs Pcdhg KD Con (contralateral), $^{*}p = 0.03$ Scrambled siRNA Inj vs Scrambled siRNA Con, two-tailed unpaired Student's t tests; $n = 4$/group; (***I***) branching points, $p =$ NS ANOVA; within culture two-way comparison $^{*}p = 0.036$ Pcdhg KD Inj vs Pcdhg KD Con, two-tailed unpaired Student's t test; $n = 4$/group]. Sholl analysis indicated that intact contralateral DRG sensory neurons treated with Pcdh γ siRNA, but not neurons with a prior axotomy injury, had greater arborization. An example is shown of an Pcdh γ Con contralateral neuron with Sholl shells placed every 10 µm from the soma center (***J***). The number of shell crossings from 20 randomly selected cells from each experiment at each 10-µm shell and averaged following a 24-h incubation is shown (***K***). Areas under the curve are quantified in ***L***, averaged per experiment [(***L***) areas $p = 0.003$ ANOVA, *post hoc*, $^{**}p = 0.0038$ Pcdhg KD Con vs Pcdhg KD Inj, $^{*}p = 0.046$ Scrambled siRNA Con vs Scrambled siRNA Inj, two-tailed unpaired Student's t test, $n = 4$ for Pcdh γ and Scrambled siRNA con (contralateral) and 5 for Pcdh γ and Scrambled siRNA Inj].

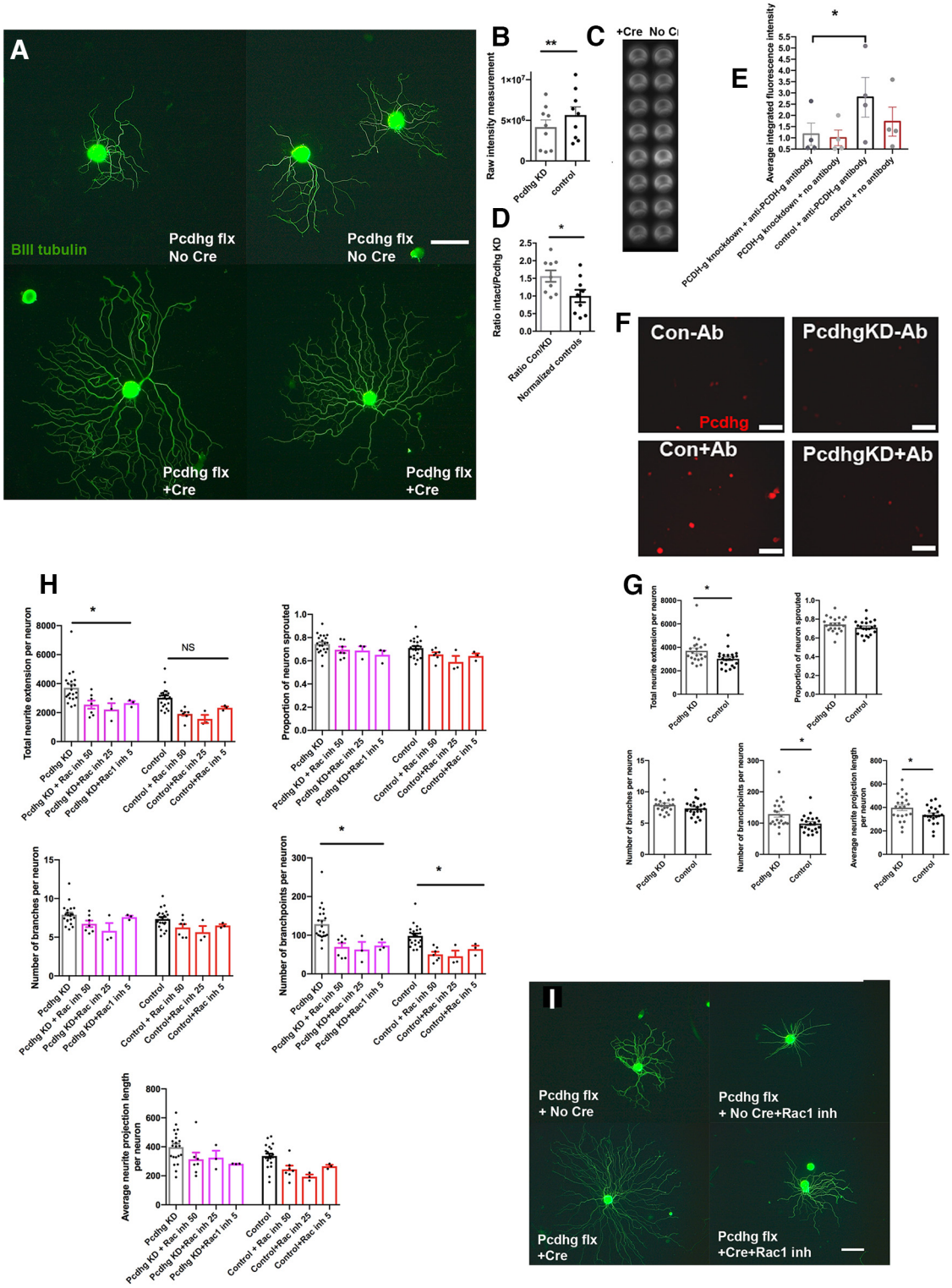

Figure 4. Knock-down in floxed Pcdh γ sensory neurons enhances axon outgrowth: naive (uninjured) mouse DRG neurons from *Pcdhg*$^{Fcon3/Fcon3}$ mice exposed to an AAV-iCre-mCherry construct or AAV-mCherry control were analyzed for neurite outgrowth. Examples of neurons exposed to control AAV-mCherry or AAV-iCre-mCherry are illustrated (***A***; scale bar = 100 μm). Knock-down of Pcdh γ was confirmed by quantitative in cell Western analysis (***B***) with an illustrated example [***C***, right; (***B***) $^{**}p = 0.0056$ two-tailed paired Student's *t* test; $n = 9$/group], also analyzed by normalization (***D***; $^{*}p = 0.032$ unpaired two-tailed Student's *t* test) and by a reduction in relative fluorescent intensity of the cells (***E***, examples in ***F***; scale bar = 100 μm; ***E***, $p = 0.0009$ repeated measure nonparametric Friedman test; $^{*}p = 0.04$ Pcdh γ KD vs control with antibody, Dunn's; $n = 4$/group). Pcdh γ knock-down cellular data are given in ***G***. AAV-iCre increased the average neurite projection length per neuron, the number of branchpoints per neuron, and the overall neurite extension per neuron. Numbers of branches and proportion of neurons with sprouting were unchanged (***G***; total neurite extension per neuron, $^{*}p = 0.02$, two-tailed unpaired Student's *t* test, $n = 21$/group; number of branchpoints $^{*}p = 0.011$, two-tailed unpaired Student's *t* test, $n = 21$/group; average neurite length $^{*}p = 0.046$, two-tailed unpaired Student's *t* test, $n = 21$; in addition, paired analysis for total extension, branchpoints and average length all $p < 0.005$). A Rac1 inhibitor dose study identifies prevention of heightened neurite outgrowth, and number of branchpoints/neurons (***H***). Control preparations has only trends, not significant, toward lesser neurite outgrowth at the 50 and 25 mg/ml, but not appreciated at 5 mg/ml (10% of the original dose). There were no differences among proportion of sprouted neurons, numbers of branches and average neurite projection length in these studies [(***H***) for Pcdh γ KD total neurite outgrowth studies ANOVA $p = 0.015$ compared with Control studies

to Pcdhγ knock-down may be growth cone/Rac1 dependent, suggesting a local action in terminal axons. We identified that rises in neurite outgrowth resulting from Cre-mediated Pcdhγ-knock-down were abrogated in the presence of the lowest dose of an applied Rac1 inhibitor NSC-23766 without impact on outgrowth of control neurites (Fig. 4*H*,*I*).

The Pcdhγs influence self and neighbor neurite crossings

In the dorsal horn of spinal cord, self-avoidance and tiling have been identified in terminals of DRG low threshold mechanoreceptive afferents (Kuehn et al., 2019). To investigate this property in DRG sensory neurons generally, we next investigated whether the phenomenon of self-avoidance was lost during Pcdhγ knock-down in both injured and contralateral cultured adult sensory neurons. Intersections were classified as requiring an approach of neurites which we interpreted as confrontations from two primary "self" branches traced to the same neuron soma. In naive uninjured contralateral adult neurons, siRNA knock-down of Pcdhγ was not associated with differences in self-intersections between self-neurites compared with Scrambled control knock-down (Fig. 5*A*–*C*). However, in a parallel experiment, using uninjured adult DRG sensory neurons from AdvCre;*Pcdhg*$^{Fcon3/Fcon3}$ mice exposed to AAV-Cre or AAV control, crossing numbers were higher overall and there was evidence of increased crossing, albeit of limited degree, in the neurons exposed to Cre with knock-down (Fig. 6).

To determine whether injury and Pcdhγ have impacts on DRG neurite self-avoidance we examined self-intersections in preconditioned neurons with Pcdhγ or Scrambled siRNA. This Pcdhγ knock-down cohort had significantly fewer intersections per cell (Fig. 5*A*). Fifty percent of injured neurons, regardless of siRNA treatment, contained less than nine intersections per cell (Fig. 5*B*), compared with the contralateral neurons. A two-way ANOVA revealed a main effect of injury ($F_{(1,837)} = 6.445$, $p = 0.01$), and a main effect of treatment ($F_{(1,837)} = 4.609$, $p = 0.03$), as well as a significant interaction between injury and treatment ($F_{(1,837)} = 5.112$, $p = 0.02$; Fig. 5*C*). We hypothesized that as the neurites grew longer, the chance of self-intersecting is higher.

To confirm, we conducted a linear regression to visualize the relationship between intersections and neurite length (Fig. 5*D*). The slope of each line (visualized in Fig. 5*E*) demonstrates how many intersections are accounted for by an increase in neurite outgrowth. We found that the injured neurons with Pcdhγ intact (Scr Inj, red line) had the steepest slope, illustrating that at higher levels of neurite outgrowth, there were more intersections per 1000 µm. Both uninjured contralateral groups (Pcdhγ siRNA Con and Scr siRNA Con) had equal slopes, and thus equal intersections per 1000 µm of neurite outgrowth. Slopes and 95% confidence intervals (Fig. 5*E*) show the Scr siRNA Inj group exhibited no overlap with any other group. We noted that injured Scr siRNA neurons exhibited fewer intersections/cell compared with the uninjured Scr control (Fig. 5*A*), but when the neurite outgrowth was taken into account, the Scr Inj neurons exhibited the most intersections/neurite growth of the four groups. This suggests a unique role for the Pcdhγs: the presence of Pcdhγ in an injured mouse appears to increase the number of intersections its neurites exhibit as the neurites grow longer.

In addition to self-avoidance, we also investigated the impacts of injury and Pcdhγ KD on tiling or neighbor interactions, by assessing the extent of interneuronal intersections per cell *in vitro*. There was a trend, albeit nonsignificant, toward greater neighbor intersections in contralateral uninjured neurons with Pcdhγ knock-down compared with Scrambled siRNA (Fig. 5*F*). With injury, while numbers of intersections were also not significantly different between Pcdhγ siRNA and Scrambled siRNA, the percentage of intersections in Pcdhγ siRNA-treated neurons significantly increased (Fig. 5*G*). The percentage of interneuronal intersections was counted when neurites from separate neurons approaching each interacted or not, as an all or none response (1 = intersection, 0 = full avoidance). There was no impact of injury itself on neighbor intersections.

We also confirmed a higher proportion of neighbor crossings in adult DRG sensory neurons from uninjured *Pcdhg*$^{Fcon3/Fcon}$ mice exposed to AAV-Cre vector compared with AAV control (Fig. 6), with differences that were more marked than self-intersections described above. Taken together, we conclude that naive uninjured Pcdhγ knock-down neurons had limited loss of self-avoidance, and more marked loss of neighbor avoidance than controls. However conditioned preinjured neurons exhibit greater self-avoidance (fewer intersections) overall but with added Pcdhγ knock-down there was lesser neighbor avoidance (more intersections) or tiling. The overall findings support the idea that Pcdhγs impact not only outgrowth and branching, but also neurite interactions.

Pcdhγ knock-down in skin *in vivo* does not impact electrophysiological or behavioral recovery after injury

To investigate whether traditional indices of regeneration might be altered by local Pcdhγ KD in skin, we studied Pcdhγ knock-down *in vivo* using siRNA following previously described methods (Christie et al., 2010, 2014; Komirishetty et al., 2021). Pcdhγ siRNA was locally administered with electroporation directly to the nerve and footpads following a sciatic nerve injury over a 28-d regeneration with evidence of ongoing knock-down of Pcdhγ mRNA in the footpad but no significant changes in DRG mRNA, indicating selective skin knock-down (Fig. 7*A*). Footpad protein expression was reduced by Pcdhγ siRNA (Fig. 7*B*,*C*). At 14 and 28 d, multifiber electrophysiological recordings (Fig. 7*D*–*G*) of ipsilateral CMAPs and SNAPs had expected postinjury declines in amplitudes and conduction velocities. However, their mean values and proportion of reappearance at both time points were comparable among the treatment groups. These findings indicated that the protocol had a local regional, but not neuronal perikayal impact.

Mechanosensitivity (Fig. 7*H*) and thermal sensitivity (Fig. 7*I*) trended toward heightened values with lower thresholds after injury (allodynia) overall in this cohort of mice, differing from other strains where significant loss of sensation may be observed. There were no differences during recovery among the groups at any of the timepoints (Figs. 7*J*,*K*).

Pcdhγ knock-down increases epidermal re-innervation and structure following injury

We next addressed what the impact of local Pcdhγ knock-down within the footpad skin might have on sensory axon reinnervation

←

ANOVA, p = NS; *post hoc* *$p = 0.029$ Pcdhγ KD vs Pcdhγ KD+Rac inh 5, Mann–Whitney two tailed; For Pcdhγ branchpoint studies ANOVA $p = 0.0018$; *post hoc* *$p = 0.015$ Pcgdhγ KD vs Pcdhγ KD+Rac inh 5 mg/ml; Mann–Whitney two-tailed; For Control branchpoint studies ANOVA $p = 0.0002$, *post hoc* *$p = 0.036$ Control vs Controls+Rac inh 5 mg/ml, Mann–Whitney two-tailed; for the Pcdhγ sprouting, and average neurite projection groups ANOVA p = NS; for all neurite outgrowth work $n = 21$ (Pcdhγ KD, Control), 7 (Pcdhγ KD or Con+RI50), 3 (Pcdhγ KD or Con+RI25), 3 (PcdhγKD or Con+RI5)]. Examples of neurons exposed to control AAV-mCherry or AAV-iCre-mCherry with or without a Rac1 inhibitor are illustrated (*I*; scale bar = 100 μm).

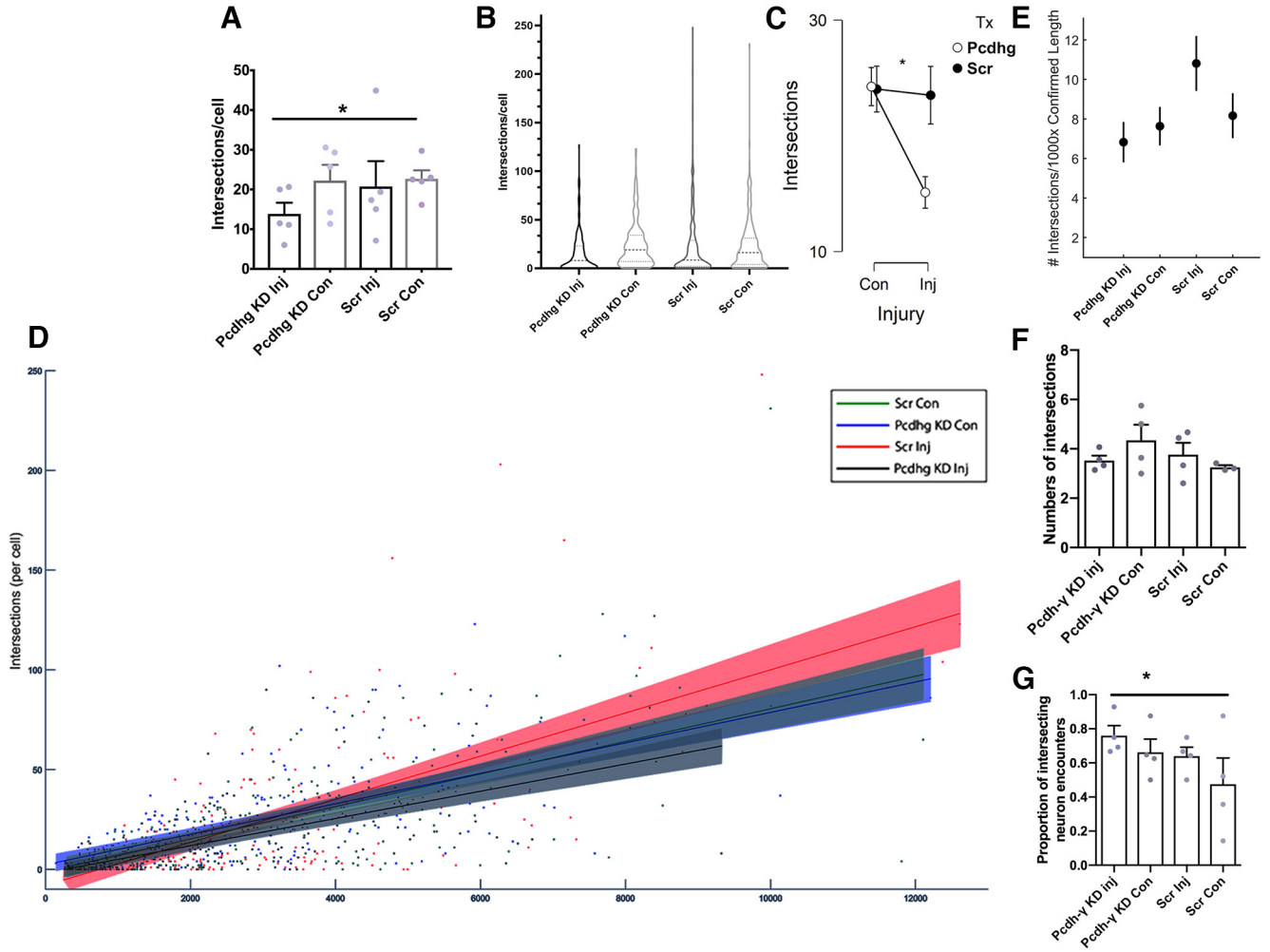

Figure 5. Injury, in the presence of Pcdh γ knock-down by siRNA, influences intraneurite and interneurite dynamics. Injury, in the presence of Pcdh γ knock-down by siRNA, influences intra and interneurite dynamics. Self-crossings or intersections were first analyzed. Following axotomy injury both injured Pcdh γ siRNA and Scrambled siRNA-treated neurons had fewer intersections per cell compared with their contralateral counterparts (***A***; number of intersections, $p = 0.031$ repeated measure nonparametric Friedman test; Pcdh γ KD Inj vs Scr Con $^*p = 0.04$, Dunn's; $n = 5$/group). Violin plot depicting that the majority of injured neurons examined contained less than nine intersections/cell (median values; Pcdh γ KD Inj: 8 intersections/cell, Scrambled siRNA Inj: 8.5 intersections/cell), compared with the contralateral neurons (***B***; median values, Pcdh γ KD Con:19 intersections/cell, Scrambled siRNA Con: 16 intersections/cell). There was a significant interaction between treatment and injury, which is likely driven by injury in the Pcdh γ KD group (***C***; $^*p = 0.02$, two-way ANOVA). We compared the relationship between intersections and neurite length in ***D***, which shows differentiation between injured groups at higher outgrowth levels (red and black lines with shaded confidence intervals). ***D***, Pcdh γ KD Inj $R^2 = 0.363$; Pcdh γ KD Con $R^2 = 0.367$; Scrambled siRNA Inj $R^2 = 0.361$; Scrambled siRNA Con $R^2 = 0.367$. Injured neurons with Pcdh γ intact (Scr Inj, red) showed a higher number of intersections per 1000 μm than neurons with Pcdh γ knocked down (Pcdh γ Inj, black). Slope values and slope confidence intervals of each group are presented in ***E*** for visualization (***E***; Pcdh γ KD Inj slope = 6.8 intersections per 1000 μm neurite growth, [5.8, 7.8]; Pcdh γ KD Con slope = 7.6, [6.7, 8.6]; Scrambled siRNA Inj slope = 10.8, [9.4, 12.2]; Scrambled siRNA Con slope = 8.2, [7.0, 9.3]). Pcdh γ KD Inj: $n = 215$, Pcdh γ KD Con: $n = 211$, Scrambled siRNA Inj: $n = 208$, Scrambled siRNA Con: $n = 207$. Interneurite intersections were also examined between two neighboring neurons. Intersections were either quantified, counting only those that were unequivocally arising from separate neurons (***F***) which were not different among the groups (*x*-axis groupings in ***E*** and ***G*** apply to ***F***). Neuron pairs were also classified as "intersecting" or "not intersecting," and a percentage of encounters that were "intersecting" was calculated (***G***; $p = 0.017$ repeated measure nonparametric Friedman test; Pcdh γ KD Inj vs Scr Con $^*p = 0.012$ Dunn's; $n = 4$/group).

at 28 d using PGP9.5 expression, a pan-axonal marker (Fig. 8*A–E*). Control Scrambled siRNA-treated hindpaws had partial reinnervation but below levels of intact uninjured contralateral hindpaws. In reinnervating hindpaws treated with Pcdh γ siRNA, there was a higher density of reinnervating fibers per mm or per length of epidermis crossing the epidermal-dermal border than in injured mice treated with a Scrambled siRNA (Fig. 8*A*,*B*). Moreover, both measures in the Pcdh γ siRNA group were similar to the innervation of control contralateral hindpaws indicating near complete anatomic axon reinvestment.

To assess axon directionality, axons classified as vertical (46–90° deviation from dermal/epidermal border) were more numerous in Pcdh γ siRNA treated mice compared with Scrambled control siRNA whereas horizontal (0–45° deviation) were similar (Fig. 8*C*,*D*). Control contralateral hindpaws and hindpaws treated with Pcdh γ siRNA had most of its axons closely spaced at 0–30 μm apart and the least number of axons with spacing at 51–200 μm, shifts in spacing indicating a relatively high innervation density. However, in mice treated with Scrambled control siRNA spacing was shifted to wider values, indicating a lower density of innervation (Fig. 8*F*). This indicated improved spacing in Pcdh γ siRNA mice (greater innervation).

We next asked whether enhanced epidermal axon plasticity involved a population of dermal axons at a fixed distance deep to the dermal-epidermal junction (axons within 50 μm of the subepidermal border) between groups (Fig. 8*G–J*). Despite a nonsignificant trend toward fewer axons in ipsilateral reinnervating

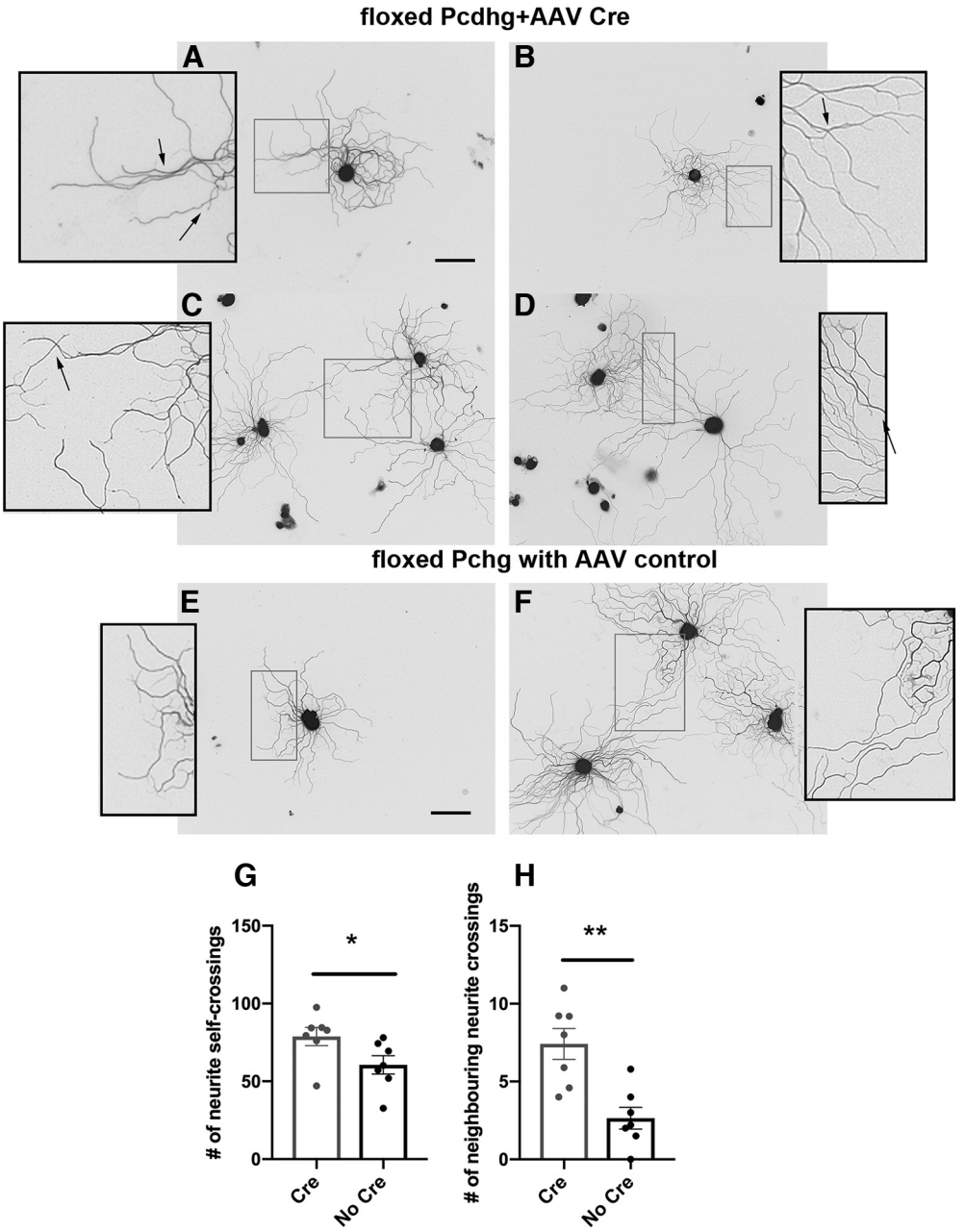

Figure 6. Knock-down in floxed Pcdh γ uninjured sensory neurons enhances self and neighbor neurite crossings. Naive (uninjured) mouse DRG neurons from *Pcdhg*$^{Fcon3/Fcon}$ mice exposed to an AAV-iCre-mCherry construct or AAV-mCherry control, were analyzed for numbers of self-crossings per neuron and number of crossings or intersections with neighboring sensory neurons. Examples of self-crossings, with a suggestion of bundling are illustrated in neurons exposed to AAV-iCre-mCherry (***A***, ***B***), boxes indicate enlarged view, whereas neurons treated with AAV-mCherry control constructs had neurites indicating a close approach to one another but no crossing (***E***). Data are given in ***G*** (*$p = 0.048$, two-tailed unpaired Student's t test, $n = 7$; $p = 0.0006$ paired analysis). Examples of neighbor crossings or intersections are illustrated in neurons exposed to AAV-iCre-mCherry (***C***, ***D***, boxes indicate enlarged view), whereas neurons treated with AAV-mCherry control constructs had neurites indicating a close approach to one another but no crossing (***F***). Data are given in ***H*** indicating a greater degree neighbor crossings in neurons treated with AAV-iCre-mCherry (***H***; **$p = 0.0021$, two-tailed unpaired Student's t test, $n = 7$; $p < 0.0001$ paired analysis; scale bars = 100 μm for ***A–F***).

hindpaws treated with Scrambled control siRNA, measurements of axons were comparable among all of the groups. Finally, we asked whether branching or arborization of afferent terminals in the epidermis were reconstituted. While both Pcdh γ and Scrambled siRNA-treated reinnervating hindpaws had fewer branches from vertical axons than intact skin, a two-way comparison suggested that these were more numerous following Pcdh γ siRNA compared with Scrambled siRNA (Fig. 8*K*,*L*). The findings confirmed that the impact of Pcdh γ knock-down was evident exclusively among distal sensory arbors that are present in the epidermis.

Hindpaw reinnervation following Pcdhγ hindpaw knock-down alters epidermal structure

We addressed whether epidermal axon reinnervation manipulated by Pcdh γ KD might have a bidirectional impact, given Pcdh γ expression within keratinocytes (Fig. 1*L–N*) and the very close relationships between axons and layered keratinocytes (Fig. 9*A–C*). The figure includes illustrations of axonal reinnervation at lower and higher power (Fig. 9*A–C*) as well as illustrations of the technique for measuring parameters as described (Fig. 9*E*,*G*, *I*). In reinnervating footpads treated with control Scrambled siRNA, there was a decline in keratinocyte DAPI stained nuclear

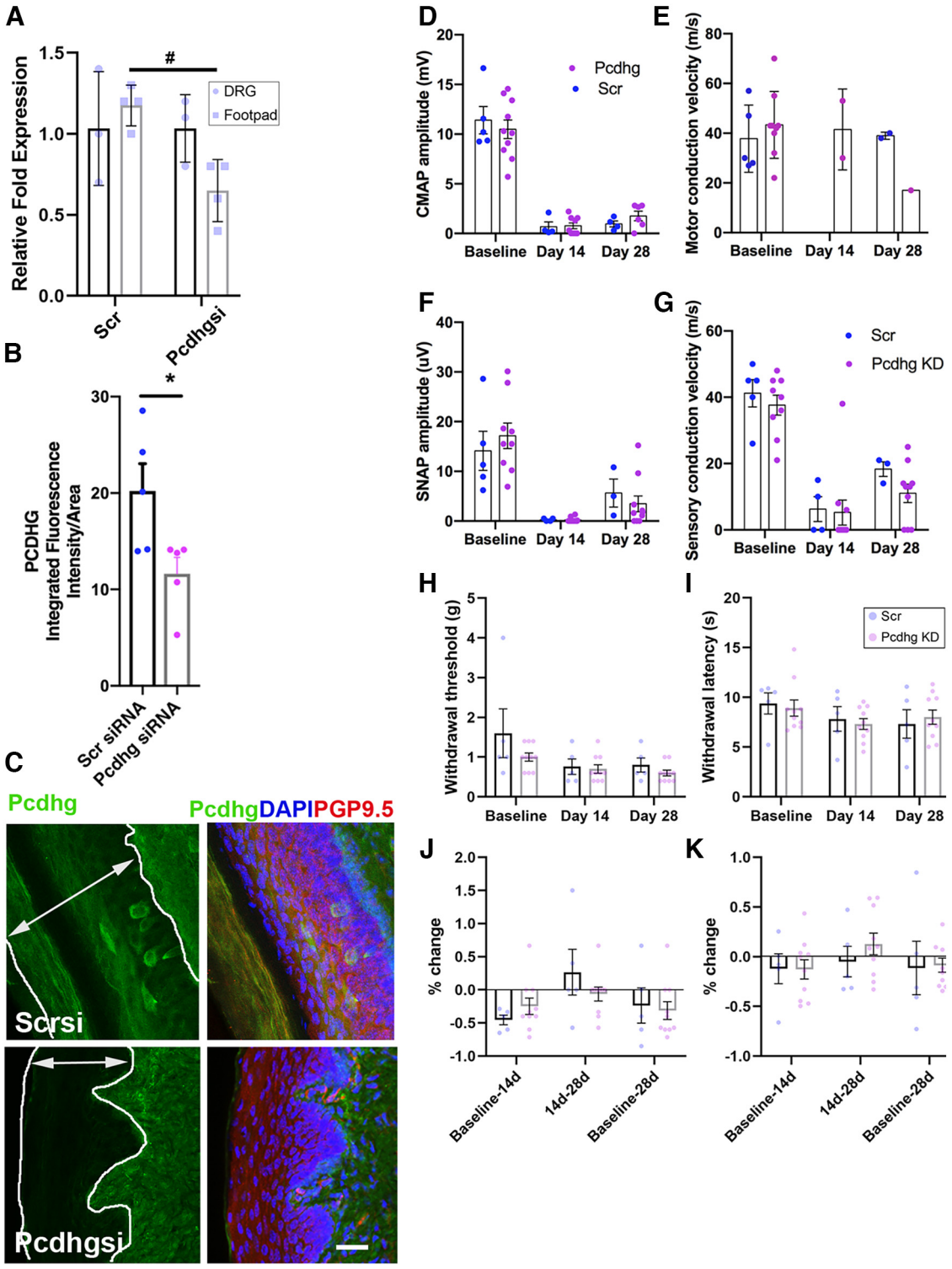

Figure 7. Pcdh γ siRNA ipsilateral to nerve injury does not alter electrophysiological or behavioral recovery. Following an ipsilateral sciatic crush injury at 28-d Pcdh γ mRNA levels measured in the footpad show a significant decline in expression in the hindpaw footpads of Pcdh γ siRNA compared with a Scrambled siRNA control groups, while DRG levels remain stable (***A***; footpad mRNA contra vs ipsi #$p = 0.026$; one-tailed Student's unpaired t test, $n = 3$ Scrambled siRNA and 4 Pcdh γ siRNA groups). Footpad epidermal protein Pcdh γ expression after Pcdh γ siRNA treatment *in vivo* measured by integrated immunohistochemical fluorescent intensity (***B***) was reduced after 28 d with examples illustrated (***C***; scale bar = 20 μm). The images show Pcdh γ (green) in the epidermis with scrambled (Scr; above) or Pcdh γ siRNA (below) without or with additional labeling for DAPI and PGP9.5. The arrows and added lines show the epidermal width. The external layer (left side) in the Scr image is external cornified keratin and the dermis is deep (right side) to the line (***B***; *$p = 0.032$ unpaired two-tailed Student's t test, $n = 5$/group). Multifiber electrophysiological measurements were conducted before injury (baseline), and again after injury at 14 and 28 d. CMAP, SNAP amplitudes, and SNAP conduction velocities were markedly reduced, as expected after injury, at both 14 and 28 d and had some evidence of recovery by 28 d but without differences between the treatment groups (***D–G***). There were nonsignificant trends toward lower withdrawal thresholds to mechanical and thermal sensation after injury, indicating allodynia, and no differences between the hindlimbs treated with Pcdh γ siRNA compared with those given Scrambled control siRNA (***H***, ***I***). The percentage change in thermal and mechanical sensation from baseline to 14 d, 14–28 d, and baseline–28 d were also similar among the groups (***J***, ***K***).

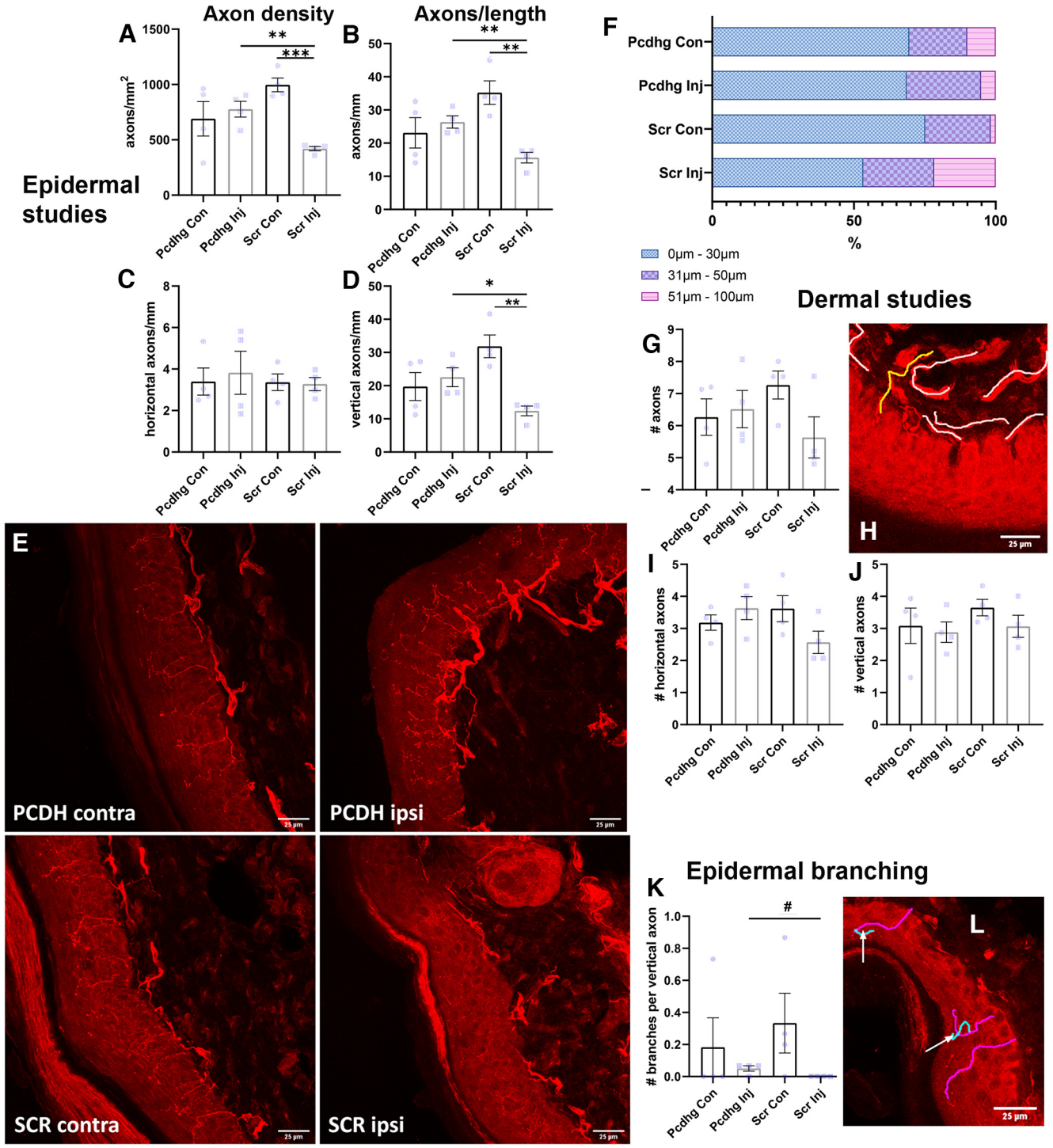

Figure 8. Pcdh γ siRNA knock-down is associated with heightened epidermal reinnervation. Analysis of epidermal innervation in footpads of hindlimbs ipsilateral and contralateral to injury (***A–E***). Epidermal fiber density and numbers of axons per length of epidermis were increased in the reinnervating Pcdh γ knock-down footpad compared with the injured Scrambled siRNA footpad [(***A***) axons per mm^2, $p = 0.006$ ANOVA, *post hoc*, $^{**}p = 0.0026$; Pcdh γ inj siRNA vs Scrambled inj siRNAi; $^{***}p < 0.0001$ Scrambled siRNA contra vs Scrambled siRNA inj, unpaired two-tailed Student's *t* tests; $n = 4$/group; (***B***) axons per mm, $p = 0.006$ ANOVA, *post hoc*, $^{**}p = 0.004$; Pcdh γ inj siRNA vs Scrambled inj siRNA; $^{**}p = 0.002$ Scrambled siRNA contra vs Scrambled siRNA inj, unpaired two-tailed Student's *t* tests; $n = 4$/group]. Axon numbers per length that were oriented $\leq 45°$ from epidermal plane (horizontal) were not different among the groups. Axons numbers per length that were oriented $>45°$ from the epidermal plane surface (vertical) were greater in reinnervated footpads with Pcdh γ knock-down (***D***; vertical axons per mm, $p = 0.0066$ ANOVA, *post hoc*, $^{*}p = 0.017$; Pcdh γ inj siRNA vs Scrambled inj siRNA; $^{**}p = 0.0017$ Scrambled siRNA contra vs Scrambled siRNA inj, unpaired two-tailed Student's *t* tests; $n = 4$/group). Representative images of footpads for each group stained with PGP9.5 are illustrated in ***E***. Reinnervating Pcdh γ knock-down footpad axons showed a denser epidermal fiber distribution, with more axons having narrower 0- to 30-µm interfiber distances compared with Scrambled siRNA Inj axons and a similar spacing distribution to contralateral control footpads (***F***). Additional forms of analysis are illustrated in ***G–L***. Dermal axon counts were made, identifying all dermal axons to within 50-µm depth from the epidermal-dermal junction (***G***, illustrated in ***H***), but also those dermal axons horizontally directed ($\leq 45°$ from the epidermal plane; ***I***, illustrated by white tracings in ***H***), or dermal axons that were vertically directed (46–90° from the epidermal plane; ***J***, illustrated by yellow tracings in ***H***). There were no differences among the treatment groups in total, horizontal or vertical dermal axons. Numbers of intraepidermal branches were analyzed and illustrated in ***K***, ***L*** (blue tracings with white arrows show examples of branches in ***L***). Numbers of branches from epidermal axons were less in reinnervated footpads compared with control contralateral intact footpads, and Pcdh γ knock-down reinnervated footpads had a trend toward more branches than those given scrambled control siRNA (***K***; number of

density. However in Pcdhγ knock-down footpads these parameters were restored (Fig. 9*D*,*E*). Keratinocyte nuclear area (μm^2) was similar among the intact contralateral footpads and the Scrambled siRNA treated reinnervating footpads but we noted a rise in nuclear area in keratinocytes from footpads exposed to Pcdhγ KD (Fig. 9*F*,*G*). We also asked whether Pcdhγ KD might be associated with closer relationships between epidermal axons and keratinocytes (Fig. 9*H–J*). There were greater numbers of keratinocyte nuclei that were in close relationship (<10-μm distance based on the estimated full keratinocyte cell diameter) to axons in contralateral intact footpads (Fig. 9*H*,*I*). Scrambled siRNA treated footpads after injury had fewer numbers of axon-keratinocyte close relationships whereas in Pcdhγ KD footpads, numbers were similar to control uninjured hindpaw footpads. However, when corrected for axon length, numbers of closely associated keratinocytes were comparable for all of the groups despite a nonsignificant trend toward a decline in both injury groups (Fig. 9*J*). Taken together, the findings indicated that Pcdhγ knock-down restored interactions between axons and keratinocytes as a function of their greater axon length.

Discussion

This study analyzed the expression and function of the Pcdhγ subcluster in peripheral neurons and skin. The overall results indicate an important impact on attenuating sensory axon growth, branching and their interactions with skin keratinocytes during reinnervation. The major findings were: (1) Pcdhγ protein and mRNA is expressed in the cytoplasm of primary sensory neurons, and in keratinocytes; (2) Pcdhγ levels in ipsilateral sensory neurons transiently decline after axotomy injury; (3) naive nonaxotomized adult sensory neurons but not those with axotomy, have rises in neurite outgrowth following Pcdhγ knock-down, that is prevented by Rac1 inhibition; (4) naive noninjured adult sensory neurons *in vitro* following Pcdhγ knock-down using AAV-Cre transfection had a limited rise in the number of self-intersections of their neurites and more robust rises in neighbor neuron intersections; (5) axotomized adult sensory neurons show an unexpected decline in self-intersections of their own extending neurites following Pcdhγ knock-down but greater numbers of neighbor intersections; (6) during regeneration after nerve injury, electrophysiological recovery in motor or sensory axons and behavioral sensory measures were not impacted by Pcdhγ knock-down; (7) epidermal reinnervation and intraepidermal branching by sensory axons was enhanced by local Pcdhγ knock-down within the skin whereas dermal reinnervation was unchanged; finally, there were also secondary structural impacts on the epidermis indicating a bidirectional impact of Pcdhγ knock-down.

Pcdhγ detection within DRGs was pan-neuronal consistent with prior reports (X. Wang et al., 2002; Prasad et al., 2008; Prasad and Weiner, 2011). Although alternate Pcdh family members were not studied, certain isoforms may be linked to specific functions through distinctive internal signaling pathways mediated by unique juxtamembrane domains (Chen et al., 2017; Li et al., 2017; Garrett et al., 2019; Carriere et al., 2020). Some isoforms are preferentially expressed in certain CNS neuron populations such as Pcdhα C2 in serotonergic neurons, and Pcdhγ A12 in granule cells (X. Wang et al., 2002; Frank et al., 2005; Chen et al., 2017). It is possible DRG neurons destined to innervate a local region or dermatome preferentially fasciculate together, guided by Pcdh isoform identity to bring them to a coordinated target destination (Chen et al., 2017; Mountoufaris et al., 2017). This would also explain how DRG projections are topographically conserved at both central (spinal cord) and peripheral (epidermal) termini. As cells may express the same isoforms on both central and peripheral projections, this would allow similar relationships with other neurons at both ends, despite arising from spatially distinct DRGs (Esumi et al., 2005; Zylka et al., 2005; Kaneko et al., 2006; Kuehn et al., 2019). Given the substantial evidence for a major role of Pcdhγ in neuron-neuron or other cell interactions, we focused on this family member.

We also observed smFISH labeling in the keratinocytes, verifying our immunohistochemical staining, which supports Pcdhγ expression in non-neuronal cells (Frank et al., 2005). While it is possible Pcdhγ is present in Schwann cells, given reports in other glial cells (Molumby et al., 2016), we did not identify convincing colabeling.

We identified an unexpected increase in outgrowth of naive, nonaxotomized, adult sensory neurons following Pcdhγ knock-down. Moreover, this heighted outgrowth involved the participation of Rac1, a growth cone GTPase that enhances lamellopodia action. Some reports show contrary declines in CNS dendritic growth and complexity with deletion of Pcdhγ (Garrett et al., 2012; Suo et al., 2012), and pyramidal neuron dendrites were noted to have enhanced growth and contacts when genetically arranged for selective expression of a Pcdhγ similar to that of their surrounding astrocytes (Molumby et al., 2016). This may indicate that an incomplete decrease in Pcdhγ isoform diversity, as might result from partial knock-down, may paradoxically increase neuronal outgrowth, facilitated by increased instances of homophilic binding. Rises in neurite outgrowth in the absence of an obvious cell-cell interaction in our dissociated sensory neurons implied intrinsic signaling, previously linked to FAK, Pyk2, PKC, or Rac1 (Suo et al., 2012; Lefebvre, 2017). While low doses of a Rac1 inhibitor prevented the rises in neurite outgrowth selectively from Pcdhγ siRNA, the inhibitor at all of the higher doses attenuated growth generally, indicating that Rac1 activation is an important arbitrator of heightened neurite outgrowth. Despite this impact on naive uninjured neurons, we found that previous axotomy prevented growth enhancement following knock-down, perhaps related to substantial declines in Pcdhγ expression after injury thereby limiting its impact. This finding, at a specific defined time point, however would not be predictive of *in vivo* growth properties during a prolonged regeneration timetable.

There may be subtle differences in the knock-down phenotype of our adult neurons exposed to siRNA compared with conditional Pcdhg deletion using an AAV-Cre vector. While the degree of overall knock-down appeared similar, neurons came from mice of differing genetic backgrounds and viral transduction of neurons, while expected to delete the gene, likely varied in the proportion of cells transduced. In the siRNA-treated neurons, control neurons were harvested from the contralateral side following injury. There were more self-crossings from naive uninjured neurons exposed to AAV-Cre but not after Pcdhγ siRNA. However, changes in self-crossings were modest, and the siRNA experiments may not have had the same fidelity to detect this change. Much more impressive was the rise in neighbor crossings, observed with both forms of knock-down, albeit

←

branches off of vertically oriented fibers per axon p = NS ANOVA; ad hoc two-way comparison #$p = 0.029$ inj Pcdhγ si vs inj Scrambled siRNA si; unpaired one tailed Student's t test with Welch's correction; $n = 4$/group).

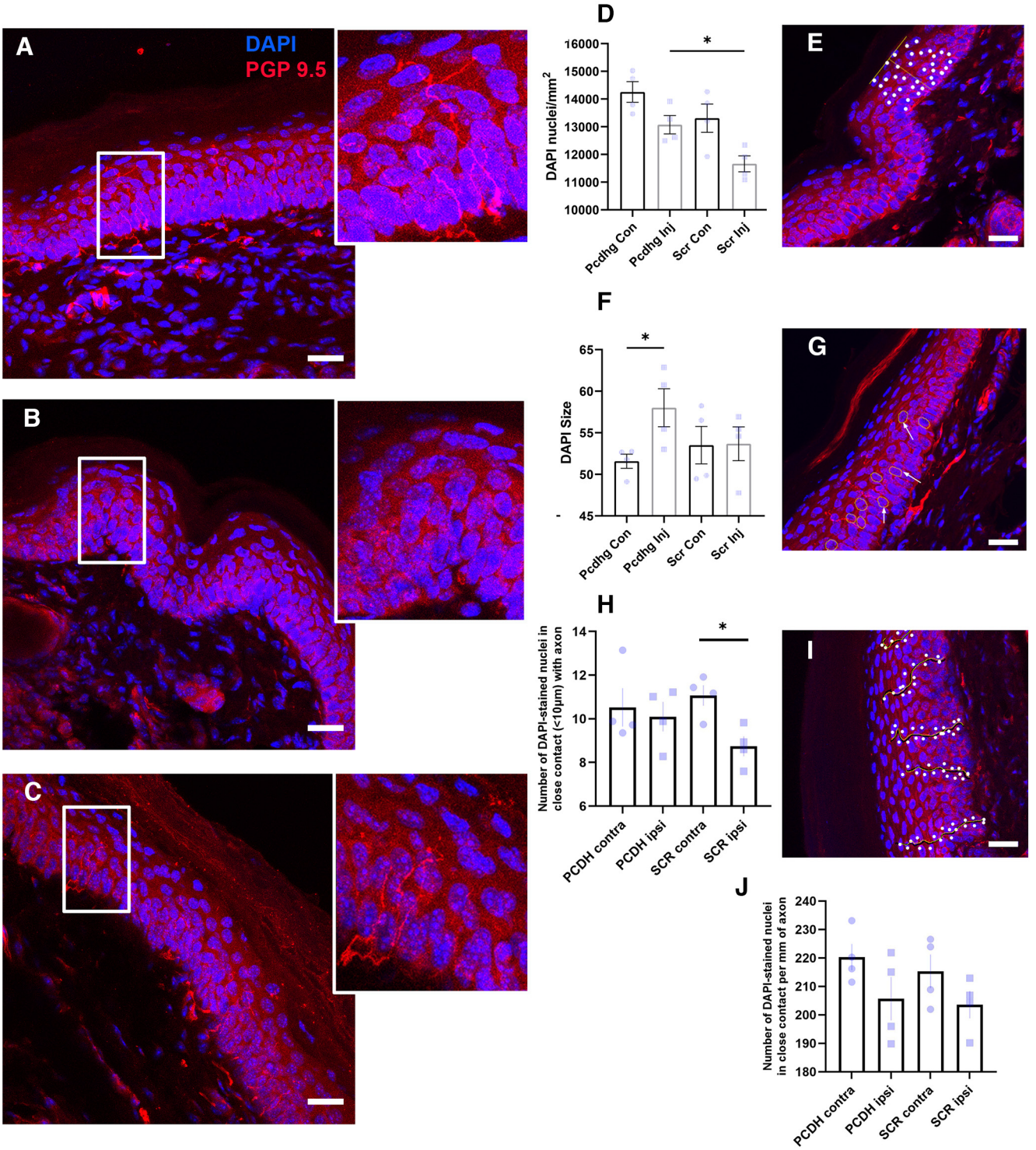

Figure 9. Pcdh γ siRNA knock-down is associated with changes in epidermal architecture. Examples of footpad sections demonstrating close relationships among keratinocytes (nuclei stained in blue) and PGP 9.5 axons (labeled in red) from intact skin (***A***), 28-d denervated skin treated with Scrambled siRNA (***B***) and 28-d denervated skin treated with Pcdh γ siRNA (***C***). Higher power insets are shown on the right of each panel. Measurements were made of the density of keratinocyte nuclei as a surrogate marker of overall keratinocyte numbers per unit area (***D***; analysis approach shown in ***E***). Control reinnervating footpads treated with Scrambled siRNA had a decline in the density of keratinocyte nuclei compared with contralateral intact footpads. Pcdh γ knock-down was associated with a preservation in nuclear density (***D***; for nuclear density, $p = 0.0037$ ANOVA, *post hoc* $^*p = 0.018$ Pcdh γ ipsi vs Scrambled siRNA ipsi, unpaired two-tailed Student's *t* test). DAPI stained keratinocyte nuclei area was measured [***F***; analysis approach using nuclear tracing (red circles and arrows) shown in ***G***]. Keratinocyte nuclear area (μm^2) was similar among the contralateral intact footpads and control Scrambled siRNA samples but there was increased nuclear area in the Pcdh γ knock-down footpads [***F***; for DAPI area, p = NS ANOVA; within mouse two-way comparison $^*p = 0.039$ Pcdh γ ipsi vs contra, unpaired ($p = 0.043$ paired) two-tailed Student's *t* tests $n = 4$/group]. Numbers of keratinocyte DAPI stained nuclei closely associated with individual epidermal axon branches were measured (***H***; analysis approach shown in ***I***). There was a decline in the numbers of keratinocytes associated with individual axons from reinnervating control footpads treated with Scrambled siRNA but not in footpads with Pcdh γ knock-down [***H***; for numbers of keratinocytes, p = NS ANOVA; within mouse two-way comparison, $^*p = 0.012$ Scrambled siRNA ipsi vs contra; unpaired ($p = 0.0082$ paired) two-tailed Student's *t* test; $n = 4$/group] When normalized for length of axons there were no differences among the groups (***J***). Scale bars = 25 μm.

only significant after injury in the siRNA group. The findings overall support the concept that Pcdhγ facilitates both self or nonself-avoidance through homophilic repulsion and its suppression favors heightened self-crossings (Lefebvre et al., 2012; Kostadinov and Sanes, 2015; Molumby et al., 2016; Chen et al., 2017; Lefebvre, 2017). However, self-crossings have largely been investigated in cells that arborize in a single plane (i.e., starburst amacrine cells, Purkinje cells; Lefebvre et al., 2012). It is not known whether peripheral sensory neurons arborize in planar orientation or are nonplanar such as hippocampal pyramidal cells where self-avoidance is not demonstrated (Garrett et al., 2012; Suo et al., 2012).

In contrast, Pcdhγ knock-down injured neurons had unexpected declines in self-intersections, especially when the extent of outgrowth was accounted for. A more likely possibility, albeit unproven, is that the role of Pcdhγ shifts in the changed protein milieu of an injured regenerating adult neuron, and that its new role is to facilitate rather than repel self axons as fasciculating sprouts in Bands of Bungner renavigate distal denervated nerve stumps on their way to targets. While we did not observe self-avoidance following injury, the story was different in neighboring cell intersections where there were heightened neighbor intersections. Overall, it appears that peripheral sensory neurons prefer tiling over self-avoidance (Grueber and Sagasti, 2010; Jan and Jan, 2010; Kuehn et al., 2019), which would be enhanced by the isoform specificity we see in specific DRG subtypes. Supernumerary sprouts by regenerating parent axons may disappear as a function of other pruning mechanisms and not require avoidance.

We delivered siRNA directly to the footpad as well as nerve, which for sensory neuron knock-down relies on retrograde transport of the siRNA to the DRG. While a similar approach has achieved knock-down in ipsilateral DRGs in previous work, this was not the case when measured at 28 d in the current work, likely requiring dose adjustment or additional electroporation to enhance uptake (Webber et al., 2011; Duraikannu et al., 2018; Komirishetty et al., 2021). Nonetheless, selective footpad Pcdhg knock-down was fortuitous because it proved informative over local events and supported the idea that local Pcdhγ interactions between axons and keratinocytes influence axon innervation and remodeling. We did not observe any impact of injury alone on footpad Pcdhγ expression. However, given the local skin impact of Pcdhγ siRNA, it is unsurprising that differential electrophysiological recovery of sensory axons was not observed. Instead, we noted a substantial increase in epidermal innervation in the injured footpad compared with a contralateral control, following Pcdhγ siRNA treatment. This degree of reinnervation is novel, as we have not encountered instances where the injured footpad at day 28 shows comparable axon innervation levels to preinjury levels, regardless of treatment. Despite heightened epidermal axon repopulation, there was no associated behavioral impact from Pcdhγ knock-down. We cannot exclude technical reasons for the behavioral findings related to the small size of mouse footpads, compared with rats, where subdivisions can be assessed more readily (Navarro, 2016). Contributions by uninjured and possibly sensitized saphenous axons innervating the medial footpad may complicate this behavioral test. It is also possible that newly arrived epidermal axons are nonetheless immature, lacking transduction properties. Despite rises in vertical axon numbers, their intraepidermal branches were reduced. More intriguing is the possibility that our observations reflect local branching from an unchanged pool of parent axons that convey unchanged sensory information centrally. In support of this idea was the lack of impact of Pcdhγ on parent dermal axon numbers and the relationship between Pcdhγ and Rac1, a growth cone molecule expected to primarily influence very distal axon terminals. The apparent impacts on keratinocytes, mainly judged by their nuclear size and density, were subtle, preliminary and of uncertain significance. However further exploration of the trophic influence of axons and Pcdhγ on detailed keratinocyte structure is a worthwhile future consideration.

With the Pcdhγ mRNA levels intact, we noted predictable outgrowth, recovery of sensitivity, and reinnervation. This might be because of the increased diversity of Pcdhγ subtypes available, imposing growth limitations on neurons. This follows the current idea that Pcdhs possess tumor suppressing abilities (Novak et al., 2008; Banelli et al., 2012; Dallosso et al., 2012; Severson et al., 2012). Given incomplete knock-down, there may ensue a decline in Pcdhg diversity, potentially facilitating increased homophilic binding, and increasing neurite extension and outgrowth, as demonstrated previously (Molumby et al., 2016). It is worth highlighting that while we observed no rise in outgrowth and decreased self-intersections in injured sensory neurons *in vitro*, we did identify increased epidermal innervation *in vivo*. However, *in vitro* studies at 3d following injury may not be comparable with events assessed *in vivo* at 28 d postinjury. Overall these findings may support a role Pcdhγ plays in the promotion of epidermal axon maturation and stabilization, possibly as a direct interaction with keratinocytes that possess synaptic-like connections with sensory axons (Talagas et al., 2020; LaMassa et al., 2021).

In conclusion, clustered protocadherins may play a significant role in regeneration, particularly in recapitulation of axon patterning after axons reach the skin. We provide evidence that Pcdhγ restricts neurite extension, perhaps Rac1 activation and influences tiling for proper, functional innervation. This is compatible with its role as a tumor suppressor, a familiar mechanism for influencing regenerative outcomes in neurons (Waha et al., 2005; Novak et al., 2008; Dallosso et al., 2009; Banelli et al., 2012; Severson et al., 2012; Mah et al., 2016; Duraikannu et al., 2019). Further understanding is critically needed, as novel molecules that enhance regeneration and the interaction of axons with their target cells could be therapeutically manipulated.

References

Allodi I, Udina E, Navarro X (2012) Specificity of peripheral nerve regeneration: interactions at the axon level. Prog Neurobiol 98:16–37.

Banelli B, Brigati C, Di Vinci A, Casciano I, Forlani A, Borzì L, Allemanni G, Romani M (2012) A pyrosequencing assay for the quantitative methylation analysis of the PCDHB gene cluster, the major factor in neuroblastoma methylator phenotype. Lab Invest 92:458–465.

Barrientos SA, Martinez NW, Yoo S, Jara JS, Zamorano S, Hetz C, Twiss JL, Alvarez J, Court FA (2011) Axonal degeneration is mediated by the mitochondrial permeability transition pore. J Neurosci 31:966–978.

Carriere CH, Wang WX, Sing AD, Fekete A, Jones BE, Yee Y, Ellegood J, Maganti H, Awofala L, Marocha J, Aziz A, Wang LY, Lerch JP, Lefebvre JL (2020) The γ-protocadherins regulate the survival of GABAergic interneurons during developmental cell death. J Neurosci 40:8652–8668.

Chandrasekhar A, Komirishetty P, Areti A, Krishnan A, Zochodne DW (2021) Dual specificity phosphatases support axon plasticity and viability. Mol Neurobiol 58:391–407.

Chen WV, Alvarez FJ, Lefebvre JL, Friedman B, Nwakeze C, Geiman E, Smith C, Thu CA, Tapia JC, Tasic B, Sanes JR, Maniatis T (2012) Functional significance of isoform diversification in the protocadherin gamma gene cluster. Neuron 75:402–409.

Chen WV, Nwakeze CL, Denny CA, O'Keeffe S, Rieger MA, Mountoufaris G, Kirner A, Dougherty JD, Hen R, Wu Q, Maniatis T (2017) Pcdhαc2 is required for axonal tiling and assembly of serotonergic circuitries in mice. Science 356:406–411.

Cheng C, Guo GF, Martinez JA, Singh V, Zochodne DW (2010) Dynamic plasticity of axons within a cutaneous milieu. J Neurosci 30:14735–14744.

Choi HMT, Schwarzkopf M, Fornace ME, Acharya A, Artavanis G, Stegmaier J, Cunha A, Pierce NA (2018) Third-generation in situ hybridization chain reaction: multiplexed, quantitative, sensitive, versatile, robust. Development 145:dev165753.

Christie KJ, Webber CA, Martinez JA, Singh B, Zochodne DW (2010) PTEN inhibition to facilitate intrinsic regenerative outgrowth of adult peripheral axons. J Neurosci 30:9306–9315.

Christie KJ, Krishnan A, Martinez JA, Purdy K, Singh B, Eaton S, Zochodne D (2014) Enhancing adult nerve regeneration through the knockdown of retinoblastoma protein. Nat Commun 5:3670.

Conforti L, Gilley J, Coleman MP (2014) Wallerian degeneration: an emerging axon death pathway linking injury and disease. Nat Rev Neurosci 15:394–409.

Dallosso AR, Hancock AL, Szemes M, Moorwood K, Chilukamarri L, Tsai HH, Sarkar A, Barasch J, Vuononvirta R, Jones C, Pritchard-Jones K, Royer-Pokora B, Lee SB, Owen C, Malik S, Feng Y, Frank M, Ward A, Brown KW, Malik K (2009) Frequent long-range epigenetic silencing of protocadherin gene clusters on chromosome 5q31 in Wilms' tumor. PLoS Genet 5:e1000745.

Dallosso AR, Øster B, Greenhough A, Thorsen K, Curry TJ, Owen C, Hancock AL, Szemes M, Paraskeva C, Frank M, Andersen CL, Malik K (2012) Long-range epigenetic silencing of chromosome 5q31 protocadherins is involved in early and late stages of colorectal tumorigenesis through modulation of oncogenic pathways. Oncogene 31:4409–4419.

Duraikannu A, Martinez JA, Chandrasekhar A, Zochodne DW (2018) Expression and manipulation of the APC-β-catenin pathway during peripheral neuron regeneration. Sci Rep 8:13197.

Duraikannu A, Krishnan A, Chandrasekhar A, Zochodne DW (2019) Beyond trophic factors: exploiting the intrinsic regenerative properties of adult neurons. Front Cell Neurosci 13:128.

Esumi S, Kakazu N, Taguchi Y, Hirayama T, Sasaki A, Hirabayashi T, Koide T, Kitsukawa T, Hamada S, Yagi T (2005) Monoallelic yet combinatorial expression of variable exons of the protocadherin-alpha gene cluster in single neurons. Nat Genet 37:171–176.

Flaherty E, Maniatis T (2020) The role of clustered protocadherins in neurodevelopment and neuropsychiatric diseases. Curr Opin Genet Dev 65:144–150.

Frank M, Ebert M, Shan W, Phillips GR, Arndt K, Colman DR, Kemler R (2005) Differential expression of individual gamma-protocadherins during mouse brain development. Mol Cell Neurosci 29:603–616.

Garrett AM, Schreiner D, Lobas MA, Weiner JA (2012) γ-Protocadherins control cortical dendrite arborization by regulating the activity of a FAK/PKC/MARCKS signaling pathway. Neuron 74:269–276.

Garrett AM, Bosch PJ, Steffen DM, Fuller LC, Marcucci CG, Koch AA, Bais P, Weiner JA, Burgess RW (2019) CRISPR/Cas9 interrogation of the mouse Pcdhg gene cluster reveals a crucial isoform-specific role for Pcdhgc4. PLoS Genet 15:e1008554.

Gerdts J, Summers DW, Sasaki Y, DiAntonio A, Milbrandt J (2013) Sarm1-mediated axon degeneration requires both SAM and TIR interactions. J Neurosci 33:13569–13580.

Grueber WB, Sagasti A (2010) Self-avoidance and tiling: mechanisms of dendrite and axon spacing. Cold Spring Harb Perspect Biol 2:a001750.

Hasegawa S, Kumagai M, Hagihara M, Nishimaru H, Hirano K, Kaneko R, Okayama A, Hirayama T, Sanbo M, Hirabayashi M, Watanabe M, Hirabayashi T, Yagi T (2016) Distinct and cooperative functions for the protocadherin-α, -β and -γ clusters in neuronal survival and axon targeting. Front Mol Neurosci 9:155.

Ing-Esteves S, Kostadinov D, Marocha J, Sing AD, Joseph KS, Laboulaye MA, Sanes JR, Lefebvre JL (2018) Combinatorial effects of alpha- and gamma-protocadherins on neuronal survival and dendritic self-avoidance. J Neurosci 38:2713–2729.

Jan YN, Jan LY (2010) Branching out: mechanisms of dendritic arborization. Nat Rev Neurosci 11:316–328.

Kaneko R, Kato H, Kawamura Y, Esumi S, Hirayama T, Hirabayashi T, Yagi T (2006) Allelic gene regulation of Pcdh-alpha and Pcdh-gamma clusters involving both monoallelic and biallelic expression in single Purkinje cells. J Biol Chem 281:30551–30560.

Komirishetty P, Zubkow K, Areti A, Ong H, Zochodne DW (2021) Delayed manipulation of regeneration within injured peripheral axons. Neurobiol Dis 155:105383.

Kostadinov D, Sanes JR (2015) Protocadherin-dependent dendritic self-avoidance regulates neural connectivity and circuit function. Elife 4:e08964.

Krishnan A, Bhavanam S, Zochodne D (2018) An intimate role for adult dorsal root ganglia resident cycling cells in the generation of local macrophages and satellite glial cells. J Neuropathol Exp Neurol 77:929–941.

Kuehn ED, Meltzer S, Abraira VE, Ho CY, Ginty DD (2019) Tiling and somatotopic alignment of mammalian low-threshold mechanoreceptors. Proc Natl Acad Sci U S A 116:9168–9177.

LaMassa N, Sverdlov H, Mambetalieva A, Shapiro S, Bucaro M, Fernandez-Monreal M, Phillips GR (2021) Gamma-protocadherin localization at the synapse is associated with parameters of synaptic maturation. J Comp Neurol 529:2407–2417.

Lefebvre JL (2017) Neuronal territory formation by the atypical cadherins and clustered protocadherins. Semin Cell Dev Biol 69:111–121.

Lefebvre JL, Zhang Y, Meister M, Wang X, Sanes JR (2008) gamma-Protocadherins regulate neuronal survival but are dispensable for circuit formation in retina. Development 135:4141–4151.

Lefebvre JL, Kostadinov D, Chen WV, Maniatis T, Sanes JR (2012) Protocadherins mediate dendritic self-avoidance in the mammalian nervous system. Nature 488:517–521.

Li Y, Chen Z, Gao Y, Pan G, Zheng H, Zhang Y, Xu H, Bu G, Zheng H (2017) Synaptic adhesion molecule Pcdh-γC5 mediates synaptic dysfunction in Alzheimer's disease. J Neurosci 37:9259–9268.

Mah KM, Houston DW, Weiner JA (2016) The γ-protocadherin-C3 isoform inhibits canonical Wnt signalling by binding to and stabilizing Axin1 at the membrane. Sci Rep 6:31665.

Meltzer S, Boulanger KC, Chirila AM, Osei-Asante E, DeLisle M, Zhang Q, Kalish BT, Tasnim A, Huey EL, Fuller LC, Flaherty EK, Maniatis T, Garrett AM, Weiner JA, Ginty DD (2023) γ-Protocadherins control synapse formation and peripheral branching of touch sensory neurons. Neuron 111:1776–1794.e10.

Moffitt JR, Zhuang X (2016) RNA imaging with multiplexed error-robust fluorescence in situ hybridization (MERFISH). Methods Enzymol 572:1–49.

Moffitt JR, Hao J, Wang G, Chan KH, Babcock HP, Zhuang X (2016) High-throughput single-cell gene-expression profiling with multiplexed error-robust fluorescence in situ hybridization. PNAS 113:11046–11051.

Molumby MJ, Keeler AB, Weiner JA (2016) Homophilic protocadherin cell-cell interactions promote dendrite complexity. Cell Rep 15:1037–1050.

Mountoufaris G, Chen WV, Hirabayashi Y, O'Keeffe S, Chevee M, Nwakeze CL, Polleux F, Maniatis T (2017) Multicluster Pcdh diversity is required for mouse olfactory neural circuit assembly. Science 356:411–414.

Navarro X (2016) Functional evaluation of peripheral nerve regeneration and target reinnervation in animal models: a critical overview. Eur J Neurosci 43:271–286.

Nguyen MQ, von Buchholtz LJ, Reker AN, Ryba NJ, Davidson S (2021) Single-nucleus transcriptomic analysis of human dorsal root ganglion neurons. Elife 10:e71752.

Novak P, Jensen T, Oshiro MM, Watts GS, Kim CJ, Futscher BW (2008) Agglomerative epigenetic aberrations are a common event in human breast cancer. Cancer Res 68:8616–8625.

Poitras T, Chandrasekhar A, McCoy L, Komirishetty P, Areti A, Webber CA, Zochodne DW (2019) Selective sensory axon reinnervation and TRPV1 activation. Mol Neurobiol 56:7144–7158.

Prasad T, Weiner JA (2011) Direct and indirect regulation of spinal cord Ia afferent terminal formation by the γ-protocadherins. Front Mol Neurosci 4:54.

Prasad T, Wang X, Gray PA, Weiner JA (2008) A differential developmental pattern of spinal interneuron apoptosis during synaptogenesis: insights from genetic analyses of the protocadherin-gamma gene cluster. Development 135:4153–4164.

Rishal I, Golani O, Rajman M, Costa B, Ben-Yaakov K, Schoenmann Z, Yaron A, Basri R, Fainzilber M, Galun M (2013) WIS-NeuroMath enables versatile high throughput analyses of neuronal processes. Dev Neurobiol 73:247–256.

Senger JB, Verge VMK, Chan KM, Webber CA (2018) The nerve conditioning lesion: a strategy to enhance nerve regeneration. Ann Neurol 83:691–702.

Severson PL, Tokar EJ, Vrba L, Waalkes MP, Futscher BW (2012) Agglomerates of aberrant DNA methylation are associated with toxicant-induced malignant transformation. Epigenetics 7:1238–1248.

Suo L, Lu H, Ying G, Capecchi MR, Wu Q (2012) Protocadherin clusters and cell adhesion kinase regulate dendrite complexity through Rho GTPase. J Mol Cell Biol 4:362–376.

Talagas M, Lebonvallet N, Leschiera R, Sinquin G, Elies P, Haftek M, Pennec JP, Ressnikoff D, La Padula V, Le Garrec R, L'Herondelle K, Mignen O, Le Pottier L, Kerfant N, Reux A, Marcorelles P, Misery L (2020) Keratinocytes communicate with sensory neurons via synaptic-like contacts. Ann Neurol 88:1205–1219.

Verge VMK, Gratto KA, Karchewski LA, Richardson PM (1996) Neurotrophins and nerve injury in the adult. Philos Trans R Soc Lond B Biol Sci 351:423–430.

Waha A, Güntner S, Huang TH, Yan PS, Arslan B, Pietsch T, Wiestler OD, Waha A (2005) Epigenetic silencing of the protocadherin family member PCDH-gamma-A11 in astrocytomas. Neoplasia 7:193–199.

Wang WX, Lefebvre JL (2022) Morphological pseudotime ordering and fate mapping reveal diversification of cerebellar inhibitory interneurons. Nat Commun 13:3433.

Wang X, Weiner JA, Levi S, Craig AM, Bradley A, Sanes JR (2002) Gamma protocadherins are required for survival of spinal interneurons. Neuron 36:843–854.

Webber CA, Christie KJ, Cheng C, Martinez JA, Singh B, Singh V, Thomas D, Zochodne DW (2011) Schwann cells direct peripheral nerve regeneration through the netrin-1 receptors, DCC and Unc5H2. Glia 59:1503–1517.

Wu Q, Jia Z (2021) Wiring the brain by clustered protocadherin neural codes. Neurosci Bull 37:117–131.

Wu Q, Zhang T, Cheng JF, Kim Y, Grimwood J, Schmutz J, Dickson M, Noonan JP, Zhang MQ, Myers RM, Maniatis T (2001) Comparative DNA sequence analysis of mouse and human protocadherin gene clusters. Genome Res 11:389–404.

Zigmond RE, Echevarria FD (2019) Macrophage biology in the peripheral nervous system after injury. Prog Neurobiol 173:102–121.

Zochodne DW (2012) The challenges and beauty of peripheral nerve regrowth. J Peripher Nerv Syst 17:1–18.

Zylka MJ, Rice FL, Anderson DJ (2005) Topographically distinct epidermal nociceptive circuits revealed by axonal tracers targeted to Mrgprd. Neuron 45:17–25.